UNIZIK JOURNAL OF ENGINEERING AND APPLIED SCIENCES (UJEAS)

Research Article

Sustainability of Dye Effluent Using Adsorptive Properties of Awka Clay: Kinetics and Modeling (RSM, ANFIS, and ANN Analysis)

Nonso C. Oguanobi, Patrick C. Nnaji, Okechukwu D. Onukwuli, Calistus N. Ude, Ephraim N. Anike, Everest U. Shedrack.

Special Issue
A Themed Issue in Honour of Professor Onukwuli Okechukwu Dominic (FAS).

This special issue is dedicated to Professor Onukwuli Okechukwu Dominic (FAS), marking his retirement and celebrating a remarkable career. His legacy of exemplary scholarship, mentorship, and commitment to advancing knowledge is commemorated in this collection of works.

Edited by
Chinonso Hubert Achebe PhD.
Christian Emeka Okafor PhD.

UJEAS

UNIZIK JOURNAL OF ENGINEERING AND APPLIED SCIENCES

UNIZIK Journal of Engineering and Applied Sciences 4(2), March (2025), 1896 - 1919
Journal homepage: https://journals.unizik.edu.ng/index.php/ujeas
PRINT ISSN: 2992-4383 || ONLINE ISSN: 2992-4391

Sustainability of Dye Effluent Using Adsorptive Properties of Awka Clay: Kinetics and Modeling (RSM, ANFIS, and ANN Analysis)

.

Nonso C. Oguanobi[1]*, Patrick C. Nnaji[1], Okechukwu D. Onukwuli[2], Calistus N. Ude[1], Ephraim N. Anike[1], Everest U. Shedrack[1].

[1].Department of Chemical Engineering, Michael Okpara University of Agriculture, P. M. B. 7267, Umudike, Abia State, Nigeria.

[2].Department of Chemical Engineering, Nnamdi Azikiwe University, P. M. B. 5025, Awka, Nigeria

*Corresponding Author's E-mail: oguanobi.nonso@mouau.edu.ng.

Abstract

Azo dyes are toxic dyes of environmental concern due to their stable aromatic structure. The research work focused on the removal of CR pollutants from aqueous solution via utilizing the adsorptive qualities of acid-modified Awka clay (AMAC). The batch adsorption was conducted to investigate the process variables effect. The adsorption mechanism was investigated. The thermodynamic properties ΔS, ΔH, ΔG, and Ea were determined. The optimum CR removal was predicted using the ANN, ANFIS, and RSM models. The maximum dye removal of 99.99% was achieved at a temperature of 323 K, an adsorbent dosage of 1 g, a contact time of 150 min, an initial dye concentration of 100 mg/l, an adsorbent particle size of 75 µm, and pH 2. A maximum equilibrium adsorption capacity of 19.9999 mg/g was obtained. The adsorption mechanism result indicates that two or more steps influence the adsorption process. Thermodynamic results suggested an endothermic, favorable, spontaneous, and physical adsorption process. The RSM model, with an R^2 of unity, is statistically more significant than the ANN and ANFIS models. A maximum reusability capacity of 97.2% was achieved after three cycles. These obtained results confirm AMAC as a reliable adsorbent for CR removal from effluents.

Keywords: adsorption, isotherm, kinetic, modelling, thermodynamics, optimization.

1. Introduction

Pollution has been a great challenge in both developed and underdeveloped countries due to the transition in society from an agricultural-based economy to an industrial economy. The revolution in the economy has been beneficial to mankind and adversely affected both aquatic and terrestrial environments, if not the ecosystem at large. The negative effect of the revolution on the economy is a result of a series of direct and indirect emissions from different industries, like the oil refining and processing industries and the dye production and consumption industries. These two industries generate wastewater containing oil, dissolved substances, color, suspended solids, chemical oxygen demand, biochemical oxygen demand, and hazardous chemicals (heavy metals) in great quantities (Oguanobi et al. 2024c). Among the many sources of industrial dye wastewater are textile, rubber, leather, paper and pulp, plastic, soap and detergent, food, paint, petrochemical, photographic, printing ink, pharmaceuticals, cosmetics, mills, and mining operations (Oguanobi et al. 2024a).

The high rate of water pollution is linked to poor waste management and a lack of strict laws regulating the discharge of sewage or inadequately treated effluents into the environment. This results in the discharge of sewage from industries into the environment without proper treatment. Recently, different physical, biological, physico-chemical, and chemical treatment techniques such as coagulation and flocculation, sonochemical degradation, adsorption, photochemical degradation, electrochemical removal, electrochemical degradation, membrane separation, bio-degradation, and anaerobic sequential process fento-biological treatment scheme, photo-fento process, and oxidation and zonation have been explored in trying to minimize the trait of water pollution from the

point source (Oguanobi et al. 2024b). All of these treatment techniques, with the exception of adsorption, have certain limitations and haven't been able to completely remove color from wastewater.

Adsorption is a unit operation and a mass transfer operation process that involves the adhesion of molecules, ions, and atoms from a liquid, dissolved solid, or gas to the surface of a material called an adsorbent. Therefore, an adsorbent is any material that is capable of removing dissolved components from an aqueous solution through the force of attraction that exists between the aqueous solution (adsorbate) and the surface of the adsorbent. This unit operation process finds great use in many industrial applications where water recovery is essential, such as textiles, rubber, leather, paper and pulp, plastic, soap and detergent, food, paint, petrochemicals, photography, printing ink, pharmaceuticals, cosmetics, etc. Activated carbon has been the conventional adsorbent for the adsorption process over time due to its uniqueness and high adsorption capacity, but the limitation of high operating costs becomes a serious concern and thereby raises the quest for a non-conventional, low-cost alternative. Different non-conventional adsorbents have been exploited, and all show the capacity to replace conventional activated carbon. Some of the previously exploited non-conventional adsorbents include modified clays (Oguanobi et al. 2018, Nayoon et al. 2022), modified biomass (Mohammed et al. 2023), red clay (Muhammed and Çiğdem 2022), eggplant biomass (Zhi et al. 2022), agricultural waste (Dal and Meenal 2022), rice bran (Mojtaba et al. 2020), and rice husk (Onu et al. 2020), clay mineral (Zineb et al. 2023, Oguanobi et al. 2024a), zeolite-based bio membrane (Sabarish et al. 2022), among others.

Nevertheless, of all the adsorbents utilized, clays demonstrate a significant adsorption capacity because of their capability to adsorb ions and molecules on both the external surface and interlayer particle sites. The processes of adsorption and desorption of organic molecules in clays are primarily influenced by the clay's surface characteristics, including its large surface area, low permeability, high retention, and cation exchange capacities. Natural clay possesses a negative structural charge, enabling it to effectively adsorb positively charged dyes, while resulting in a lower adsorption capacity for anionic dyes (Mahammedi and Benguella 2016). The natural high adsorption strengths of clay can be further enhanced through modification. Modification of clay creates a positively charged structure, which also allows the adsorption of anionic dyes (negatively charged dyes). Most works on CR dye removal have focused on studying the influence of these factors using the one-factor-at-a-time method, which is cumbersome, time-consuming, and cannot satisfactorily predict the optimum point of process variables.

RSM is a model used to generate a mathematical model that can satisfactorily give the optimum parameters for operating a process. It helps in the simultaneous examination of process variables that affect a process, even in the presence of complex interactions. RSM only needs small experimental runs to predict an optimum condition. ANN uses artificial neurons to process information. It is used to evaluate complex nonlinear problems with sizable data sets. It also analyzes problematic data sets that are difficult to tackle ordinarily. ANFIS is a kind of artificial intelligence model or concept that utilizes the learnings of fuzzy logic and neural networks to generate a hybrid model that yields an effective and precise result. ANFIS is applicable to both linear and nonlinear systems with a great level of accuracy. It is also a kind of ANN that is based on a Takagi-Sugeno fuzzy inference system (Gonzalez et al. 2020). The objective of this work was to study the effect of acid activation on the adsorptive properties of Awka clays on the removal of pollutants from Congo red dyes from an aqueous solution. It also utilizes artificial intelligent optimization models such as response surface methodology (RSM), artificial neural networks (ANN), and adaptive neuro-fuzzy inference systems (ANFIS) in modeling and predicting the optimum removal of CR dye from wastewater.

2.0 Materials and methods

The primary raw material used in this project was milk-colored clay sourced from Okpuno village in Awka South Local Government Area of Anambra State, Nigeria. Secondary raw materials, which were of analytical grade, were obtained from Bridge Head Market in Onitsha, Anambra State. All the solutions utilized were prepared using distilled water.

2.1 Acid activation of clay sample

The clay material for activation was sun-dried for three days and pulverized using a laboratory mortar and pestle. The mesh clay sample was sieved using 50 µm particle-size dry test sieves. The sieved clay sample was mixed with HCl in a conical flask in a w/v ratio of 1:6 (200g of meshed clay sample was dissolved with 1200 ml of the prepared acid) and allowed for 24 hours. The slurry was filtered after 24 hours to separate the clay from the acid. The obtained clay residue was washed with distilled water until a neutral pH point was reached with a pH indicator. The

neutral clay slurry was dried at an oven temperature of 80 ^{o}C for 240 seconds (4 hours). The obtained dried activated sample was crushed, sieved using 50µm particle-size dry test sieves, and stored in a desiccator until used.

2.2 Characterization

The activated and raw clay samples were analyzed to determine the functional group present and observe surface morphologies. The functional group analysis known as Fourier Transform Infrared (FTIR) analysis, was performed using a Shimadzu spectrophotometer model S8400, with samples prepared via the conventional KBr disc method. Additionally, the surface morphology was examined through Scanning Electron Microscope (SEM) analysis, conducted using a Joel scanning electron microscope model JSM 6400, which utilized a gold film coating around 20–25 angstroms thick.

2.3 Batch Adsorption Studies

Batch adsorption experiments were carried out to examine how various parameters such as adsorbent particle size, adsorbent dosage, initial concentration of dye, adsorption duration, pH, and temperature affect the uptake of CR dye by modified clay adsorbents. A stock CR solution was created by dissolving a specific amount of dye crystals in distilled water, which was then diluted to achieve the desired initial concentration range of 100 to 500 mg/L. The pH of the solution was adjusted using either 0.1N HCl or NaOH. The resulting effect of the studied process variables on CR uptake was determined using a UV-visible spectrophotometer for color removal, a conductivity meter for total dissolved solids (TDS) and electrical conductivity (EC) removal, and a chemical oxygen demand analyzer for chemical oxygen demand (COD) removal.

2.4 Equilibrium/isotherm studies

The equilibrium adsorption test was performed by introducing a fixed amount of adsorbent into separate 200ml glass containers containing various concentrations of CR dye solution at a consistent pH. The mixtures were then placed on magnetic stirrers maintained at a set temperature for 150 minutes to ensure equilibrium was established. Subsequently, the equilibrium dye concentration was measured using a UV-visible spectrophotometer.

At equilibrium, dye uptake "qe" (mg g^{-1}), was evaluated using expression of equation 1

$$qe = \frac{(C_o - C_e)V}{m} \quad (1)$$

Percentage dye uptake was evaluated using equation 2.

$$\% \text{ Adsorption} = \frac{(C_o - C_e)}{C_o} \times 100 \quad (2)$$

Where C_o and C_e(mg L^{-1}) were initial and equilibrium dye concentrations respectively, while V and m were the volume of the solution in liter and the mass of dry sorbent used in gram.

The adsorption isotherm is of paramount importance in any adsorption system because it describes the relationship between the adsorbate and adsorbent. In this research work, seven isotherm models were employed: the Langmuir, the Freundlich, the Temkin, the Vieth-Sladek, the Dubinin-Redushkevich, the Redlich-Peterson, and the Jovanovic, with their expressions (non-linearized forms) listed in equations 3–8. The parameters of each model provide vital information on the adsorption mechanisms, surface properties, and adsorbent affinity.

Langmuir adsorption isotherm

Langmuir isotherm expression describes adsorption homogeneity (homogeneous adsorption) as a process where all active sites have even energies and indistinguishable affinity for adsorbate onto the surface without the migration of molecules between localized surfaces. The non-linearized form of the Langmuir model can be expressed as follows:

$$q_e = \frac{Q_m K_L C_e}{1 + K_L C_e} \quad (3a)$$

Where q_m (mg/g) is Langmuir adsorption capacity constants, K_L (L/mg) is Langmuir energy/affinity of adsorption constants, C_e (mg/L) is the equilibrium concentration, and q_e (mg/g) is the amount of dye adsorbed at equilibrium.

When the K_L value is high (greater than 1), it indicates that the adsorbate molecules have a high affinity for the adsorbent surface (strong adsorption). A K_L value of unity (K_L = 1) implies that the adsorption process is at equilibrium, with no significant preference for adsorption or desorption. When K_L is greater than zero but less than unity (0 < KL < 1), it indicates that the gas molecules have low affinity for the adsorbent (weak adsorption). Finally, a K_L value of zero (K_L = 0) implies that there is no interaction between the adsorbate and the adsorbent (no adsorption).

The essential feature of the Langmuir isotherm was expressed by means of R_L, a dimensionless constant referred to as the separation factor or equilibrium parameter. R_L is calculated using the expression of equation 3b.

$$R_L = \frac{1}{1 + K_L C_o} \quad (3b)$$

The value of R_L classifies the adsorption process into the following categories: unfavorable (R_L >1), linear (R_L =1), favorable (0<R_L<1), or irreversible (R_L=0).

Freundlich adsorption isotherm

The Freundlich model presumes that the adsorption process occurs on heterogeneous solid surfaces (non-uniform surfaces with a varying range of adsorption energies). The isotherm explains the relationship between the pressure or concentration of the adsorbate at a constant temperature and the quantity of adsorbate adsorbed onto an adsorbent (a solid surface). The non-linearized form of the Freundlich model can be expressed as follows:

$$q_e = K_F C_e^{\,1/n_F} \quad (4)$$

Where C_e (mg/L) is the equilibrium concentration, q_e (mg g^{-1}) is the amount of dye adsorbed at equilibrium, K_F is Freundlich adsorption capacity and affinity constants, and n is the Freundlich adsorption intensity and mechanism constants, $1/n_f$ is a measure of the surface heterogeneity of the adsorption site.

When the n value is close to unity (1), it signifies that the adsorption sites have uniform energies, thereby suggesting a more homogeneous solid surface. This outcome certifies that the adsorption process will be better suited to BET or Langmuir isotherms. When the n value is "n < 1 or n > 1," it indicates that adsorption sites have non-uniform energies, which makes the surface more heterogeneous. This outcome certifies that the adsorption process will be best described by the Freundlich isotherm model, which is better suited to heterogeneous surfaces (adsorbents with varying adsorption energies across the surface). The n_f value within the range of 1<n_f<10 indicates a favorable and physical adsorption, whereas any value outside the range of 1<n_f<10 suggests a linear and chemical process. When the K_F value is high, it indicates a greater affinity of the adsorbate for the adsorbent, which leads to a higher adsorption capacity of the adsorbent, whereas a smaller value of K_F suggests a weaker affinity of the adsorbate for the adsorbent, resulting in poor adsorption capacity.

Temkin adsorption isotherm

The Temkin adsorption isotherm presumes that the heat of adsorption is constant and decreases linearly with coverage as a result of adsobate-adsorbent interaction on the surface. This model is more suited to real-world processes compared to the Langmuir model, which assumes a uniform energy distribution of adsorption sites and monolayer adsorption. The non-linearized form of the Temkin model can be expressed as follows:

$$q_e = \frac{RT}{a_T} \ln(A_T C_e) \quad (5)$$

Where a_T is Temkin constant related to the heat of adsorption and the coverage of the surface, A_T (l/g) is the equilibrium binding constant related to the maximum binding energy, R is the universal gas constant (8.314 J/mol K), T is the temperature in Kelvin, C_e (mg/L) is the equilibrium concentration, q_e (mg g^{-1}) is the amount of dye adsorbed at equilibrium.

When the value of a_T is high, it indicates a greater decrease in adsorption energy with increasing surface coverage, which means stronger interactions between the adsorbate and the adsorbent. A higher value of A_T indicates a broader distribution of adsorption energies, suggesting that the adsorption process involves various energy levels.

Dubinin-Radushkevich (D-R) adsorption isotherm

The Dubinin-Radushkevich isotherm model postulates that adsorption occurs due to the formation of indistinguishable energy wells within the porous structure of the adsorbent. This empirical model is used to represent the adsorption mechanism on surfaces with variability in adsorption energies using a Gaussian distribution of photon energy. The non-linearized form of the Dubinin-Radushkevich model can be expressed as follows:

$$q_e = Q_m \exp\left(-b_{DR}\left[RT\, ln\left(1 + \frac{1}{C_e}\right)\right]^2\right) \quad (6)$$

Where Q_m (mg/g) is the maximum adsorption capacity constants, C_e (mg/L) is the equilibrium concentration, q_e (mg g^{-1}) is the amount of dye adsorbed at equilibrium. b_{DR} is a constant related to the adsorbent's structural characteristics and the energy distribution of the adsorption sites.

The adsorption mechanism is being examined through the mean free energy "E" value obtained from D-R model. The D-R model constant b_{DR} relates to the mean free energy of adsorption through the expression of equation 6b.

$$E = \frac{1}{\sqrt{2b_{DR}}} \quad (6b)$$

When the b_{DR} value is small, it suggests a narrow energy distribution and probably a possible homogeneous system, whereas a larger value of b_{DR} indicates a broader energy distribution and a possible heterogeneous system.

Vieth-Sladek (V-S) adsorption isotherm

The Vieth-Sladek isotherm is an extension of the Langmuir adsorption isotherm, but incorporates a second term that account for the interaction between adsorbed molecules. This empirical model describes the adsorption process in terms of both multilayer and monolayer adsorption. In multilayer adsorption, adsorbate molecules adsorb onto the solid surface forms multiple layers on top of each other, unlike the D-R model, which focus only on localized energy wells within the porous structure. The non-linearized form of the Vieth-Sladek model can be expressed as follows:

$$q_e = K_{vs}C_e + \frac{Q_m B_{vs} C_e}{1 + B_{vs}C_e} \quad (7)$$

Where Q_m (mg/g) is Vieth–Sladek adsorption capacity constants, C_e (mg/L) is the equilibrium concentration, q_e (mg g^{-1}) is the amount of dye adsorbed at equilibrium, k_{vs} is the rate constant for the adsorption reaction, which depends on temperature (it describes the adsorption process's affinity for the adsorbent), and B_{vs} is Vieth–Sladek constants related to the rate of the adsorption and desorption reactions (it describes the adsorption process's behavior and the interaction between adsorbed molecules).

A high value of k_{vs} signifies that the adsorbent has a strong affinity for the gas molecule, whereas a low value indicates weak interaction. A high value of B_{vs} suggests strong interaction between adsorbed molecules, whereas a low value indicates poor interaction.

Redlich–Peterson (R-P) isotherm

The Redlich-Peterson isotherm model incorporates the feature of Freundlich and Langmuir, which signifies that it describes the adsorption on both heterogeneous and homogeneous surfaces. Redlich-Peterson invents this empirical equation to shed more light on the adsorption behavior of real systems, which deviate from the simplified presumptions made individually by the Freundlich and Langmuir isotherms. The non-linearized form of the R–P model can be expressed as follows:

$$q_e = \frac{K_R C_e}{1 + a_R {C_e}^{g}} \quad (8)$$

Where C_e (mg/L) is the equilibrium concentration, q_e (mg g^{-1}) is the amount of dye adsorbed at equilibrium, K_R (L/g) is constant related to the adsorption capacity and affinity of the adsorbent, a_R (L mg^{-1}) is constant related to the adsorption capacity, and g (dimensionless) are the Redlich–Paterson constant. The values of g fluctuate between 0 and 1. A low g value (g tends to zero) suggest heterogeneous adsorption characteristics of Freundlich isotherm (Henry's law), while high g value very close to unity signify homogeneous or monolayer adsorption characteristic of Langmuir isotherm. Additionally , the g value helps to interpret the extent to which a gas digress from ideal gas behavior, with higher values suggesting closer adherence to ideal gas behavior and lower values suggesting more significant deviations due to stronger intermolecular forces.

When the a_R value is high, it indicates the adsorbent has a good ability to adsorb and retain more adsorbate molecules at a given temperature, whereas a low value signifies poor adsorption and retaining ability of the adsorbent. When the K_R value is high, it indicates the adsorbent has a great adsorption capacity and affinity for the adsorbate, whereas a low value signifies poor adsorbent adsorption capacity and affinity for the adsorbate.

Jovanovic adsorption isotherm

The Jovanovic isotherm model is designed based on the assumptions of the Langmuir isotherm model but assumes surface adsorption and zero correlation between molecules. This empirical model permits some mechanical contact between the adsorbent and the adsorbate and accepts surface vibration of an adsorbed species. It also presume adsorption with both mobile and confined monolayers without lateral contact. Furthermore, the Jovanovic isotherm model equation simplifies to Freundlich isotherm (Henry's law) at low concentrations and can reach the saturation limit at high concentrations. The non-linearized form of the Jovanovic model can be expressed as follows:

$$q_e = Q_m(1 - exp^{-K_J C_e}) \quad (9)$$

Where q_m (mg/g) is Jovanovic adsorption capacity constants, C_e (mg/L) is the equilibrium concentration, q_e (mg g^{-1}) is the amount of dye adsorbed at equilibrium. K_J (L mg^{-1}) is the equilibrium constant of Jovanovic isotherm and it represents the adsorption affinity of the adsorbate for the adsorbent. It also helps to determine the extent of adsorption at different concentrations.

2.5 Kinetic Studies

In kinetic experiments, aqueous samples were taken at different time intervals to determine the uptake of dye at any preset time t.

At time t, dye uptake "qt" (mg g^{-1}) was evaluated using equation 10

$$qt = \frac{(C_o - C_t)V}{m} \quad (10)$$

Where C_t is dye concentration at any time t.

Adsorption kinetics is a very vital aspect of the adsorption system, which sheds light on the mechanism of adsorption and the adsorption dynamics in relation to time. In this research work, nine kinetic models were employed: the pseudo-first order, the pseudo-second order, the Elovich, the pseudo-nth-order model, the Avrami, the fractional power, intra-particle diffusion, the Bangham pore diffusion, the liquid film, and the Boyd models. The liquid film, Bangham pore diffusion, intra-particle diffusion, and Boyd model were proposed to identify the rate determining step of the adsorption.

Pseudo-first-order model (PFO)

The pseudo-first-order kinetic postulates that the rate of the reaction appears to depend on the concentration of one reactant, but in reality, it may involve other factors as well. The pseudo-first-order kinetic model is an empirical method used to analyze the rate of a chemical reaction or other process. The model is called "pseudo" because it may not precisely replicate a true first-order reaction, but rather, it is a simplified approach used to estimate the reaction kinetics. Additionally, this model is very useful when one of the reactants is present in excess and its concentration does not significantly change during the reaction; therefore, the model is suitable for analyzing reaction kinetics and understanding the factors affecting the reaction rate. The non-linearized form of the pseudo-first-order model can be expressed as follows:

$$q_t = q_e[1 - exp(K_1 t)] \quad (11)$$

Where q_e (mg/g) is the amount of adsorbate adsorbed at equilibrium, q_t (mg/g) is the amount of adsorbate adsorbed at time t. K_1 (min^{-1}) is the adsorption rate constants for pseudo-first-order.

Pseudo-second-order model (PSO)

The pseudo-second-order kinetic theory postulates that the concentration of the adsorbate and the product of the remaining accessible adsorption sites determine the rate of reaction. The pseudo-second-order model is an extension of the conventional second-order kinetic model, and it gives more detailed knowledge to chemical systems where the reaction rate depends on the surface coverage of adsorbed species. This kinetic model also provides a more detailed image of overall kinetics than the first-order model, especially when the adsorption process is multi-step. The non-linearized form of the pseudo-first-order model can be expressed as follows:

$$q_t = \frac{K_2 q_e^2 t}{1 + K_2 q_e t} \quad (12)$$

Where q_e (mg/g) represent the amount of adsorbate adsorbed at equilibrium, q_t (mg/g) denotes the amount of adsorbate adsorbed at time t, K_2 $gmg^{-1}min$ were the adsorption rate constants pseudo-second-order.

Elovich model

The Elovich kinetic theory postulates that the adsorbent surfaces are energetically heterogeneous. This model presumes that the adsorption kinetics will not be affected by interactions between the adsorbed and desorption ions, even at low surface coverage. The non-linearized form of the pseudo-first-order model can be expressed as follows:

$$q_t = \frac{1}{B}\ln(1 + ABt) \quad (13)$$

Where q_t (mg/g) is the amount of adsorbate adsorbed at time t, A is the Elovich constant for the initial adsorption rate, and B is the Elovich desorption constant.

When the value of A is high, it suggests a faster initial adsorption rate, meaning that the adsorbent has a high affinity for the gas molecule, whereas a smaller value of A indicates a slow initial adsorption rate. A higher value of B suggests high adsorption capacity, which means that the adsorbent surface cannot easily desorbed the adsorbate molecules, whereas a small value of B indicates poor adsorption capacity.

Pseudo-nth Order (PNO)

The pseudo-nth-order kinetic model is an empirical model used to analyze chemical systems where the reaction order is not naturally an integer, and it's an extension of the first- and second-order kinetic models. The model can be applied to different types of reactions, which include heterogeneous and homogeneous reactions. Additionally, the pseudo-nth-order kinetic model can also be applied to reactions where the order of reaction cannot be easily determined, and it can also analyze and predict the behavior of different reactions, which include mass transport processes, all catalyzed reactions, and electrochemical reactions. The non-linearized form of the pseudo-first-order model can be expressed as follows:

$$q_t = q_e - [q_e^{1-n} - (1-n)K_n t]^{1/(1-n)} \quad (14)$$

Where q_e (mg/g) is the amount of adsorbate adsorbed at equilibrium, q_t (mg/g) is the amount of adsorbate adsorbed at time t. K_n ($gmg^{-1}min$) were the adsorption rate constants for pseudo-nth-order; n is the order of reaction.

When the value of n is high (n > 1), it indicates that the rate of reaction of the reactant concentration is likely to change, whereas a smaller value of n (0 < n < 1) suggests that the reaction rate of the reactant concentration is unlikely to change. A value of n = 1 represents a first-order reaction, while n = 0 represents a zero-order reaction. A

high k value suggests a faster reaction rate, whereas a smaller value indicates a slower reaction rate. The rate constant can be used to calculate the half-life of the reaction or the time required for the reaction progress variable (x) to reach a specific value.

Avrami model

The Avrami kinetic model presumes that adsorbent surface possesses random nucleation sites across the reaction surface. This model evaluates changes in kinetic parameters as function of temperature and reaction time. The non-linearized form of the Avrami model can be expressed as follows:

$$q_t = q_e\{1 - \exp[-(K_{AV}t^{n_{AV}})]\}$$

Where q_e (mg/g) is the amount of adsorbate adsorbed at equilibrium, q_t (mg/g) is the amount of adsorbate adsorbed at time t, K_{AV} is the Avrami constant, which depends on the reaction mechanism and the system's properties. It is dimensionless and typically ranges between 0 and 1, n_{AV} is the Avrami exponent, which depends on the spatial dimension and the geometry of the growing phase. It can be a fraction or an integer, and its value determines the shape of the reaction progress curve, and t is time which is the independent variable in this equation.

Fractional power model

The fractional power kinetic model is a modified form of the Freundlich model. This empirical model calculates the exact rate of adsorption at a unit time using the model product's constant. The non-linearized form of the pseudo-first-order model can be expressed as follows:

$$q_t = Kt^V \quad (15)$$

Where q_t (mg/g) is the amount of adsorbate adsorbed at time t, this parameter "t" should not contain a value equal to zero to prevent infinite value. K(mg g-1) is the fractional power constant and v is the fractional power rate constant.

2.6 Adsorption Thermodynamics

Thermodynamics studies were to determine the energy changes involved in the adsorption. Thermodynamic parameters are calculated using the following equations

$$\Delta G^0 = \Delta H^0 - T\Delta S^0 \quad (16)$$

$$\Delta G^o = -RT \ln K_c \quad (17)$$

Where $K_c = \frac{C_s}{C_e}$ (17a)

$$\ln K_c = \left(\frac{\Delta S}{R}\right) - \left(\frac{\Delta H}{RT}\right) \quad (18)$$

Where ΔG^o, ΔH, ΔS are the standard; Gibbs free energy change, enthalpy change (heat of reaction) and entropy change, respectively. $K_c$is the equilibrium constant, C_s is the equilibrium concentration of CR on solid (adsorbent (mg/L)), R is the general gas constant (8.314J/mol/K) and T is adsorption temperature on Kelvin scale.

2.6.1 Activation energy

The nature of adsorption process can be inferred from the level of activation energy. The Arrhenius rate expression of equations 19 and 20 were used to evaluate the activation energy of adsorption.

$$K_A = Ae^{-Ea/RT} \quad (19)$$

$$InK_A = InA - \frac{Ea}{RT} \quad (20)$$

Where Ea is the Arrhenius activation energy (KJ/mol) K_A is a pseudo-second-order rate constant of adsorption (g/mg min), R is the universal gas constant (8.314J/molK) and T is the absolute solution temperature (k). Ea Can be calculated from the plot of InK_A versus 1/T.

2.7 RSM modeling

Design expert version 13 was used in both the design and the RSM-CCD analysis. The experiment was designed using a central composite design (CCD) with five factor levels as shown below in Table 1. RSM uses data obtained from design of experiments and statistical modeling technique to solve multi-variant problems (Venkatesh and Karthikeyan 2018).

Table 1: Five factor levels of the independent variables

Process parameter	+α	+1	0	-1	-α
Temperature (°C)	54.1421	50.00	40.00	30.00	35.8579
Concentration (mg/l)	582.843	500.00	300.00	100.00	17.1573
pH	12.864	11.00	6.5	2	0.1360
Time (mins)	69.3198	60	37.5	15	5.6819

The independent variables used were temperature, pH, concentration and time while the actual response (percentage adsorbed) was the dependent variable.
The number of data sets for RSM-CCD experiment can be evaluated using expression of equation 21 (Arulkumar et al. 2011).

$$Q = 2^q + 2q + q_c \quad (21)$$

Where q is the number of input factors and 2^q, 2q and q_c represents the: factorial points, axial points, and center points.

2.8 ANN modeling

Artificial neural networks (ANN) were used to model and analyze the percentage of CR dye adsorbed using the neural network toolbox of MATLAB R2021. The weighted inputs that arrive at each neuron in a biological system are processed through a nonlinear activation function to create an output signal (Manpreet et al. 2011).
The data sets used in RSM-CCD analysis were doubled and used in the ANN for accurate modeling process. The validation, training, and testing data sets each received a randomly assigned percentage of 15%, 70%, and 15% of the total data sets. The ANN architecture comprises the input nodes, hidden neuron layers, and output nodes.
To prevent over-fitting and a decrease in the convergence rate, the optimal number of hidden layers was established by iteration (Mingyi et al. 2017).

2.11 ANFIS modeling

ANFIS model was used to model and predict the optimum CR dye adsorbed, through Mathworks Inc. R2021. The ANFIS is represented as a five-layered network using the fuzzy inference system (FIS) concept. Temperature, concentration, time, and pH are the process variables that the first layer of the fuzzy system network accepts as inputs. The fuzzy rules were chosen in the second layer node and passed on to the third layer so that the activity rules could be normalized.
The fourth layer accepts the nodes, converges the parameters, and sends them as a single output layer (percentage of CR adsorbed) to the fifth layer (Bahman et al. 2018). A hybrid optimization approach was applied with zero error tolerance.

2.12 Comparative analysis of RSM, ANN, and ANFIS models

The actual CR adsorption values were compared to the predicted adsorption values by RSM, ANN, and ANFIS and subjected to statistical error indices. Five out of the seven statistical error functions given in Table 2 were used for comparative analysis. The normalized standard deviation, Chi-square test, average percentage error, and root mean square error functions were statistical error tool used to determine the best-fit equilibrium and kinetic model for the system.

Table 2. Statistical error functions used

Error function	Equations	Eqn Num.
Correlation coefficient	$R^2 = 1 - \frac{\sum_{i=1}^{N}(\mathrm{M_{exp}} - \mathrm{M_{pre}})^2}{\sum_{i=1}^{N}(\mathrm{M_{exp}} - M_m)^2}$	(23)
Average percentage error	$APE = \sum_{i-1}^{N} \frac{\left\|q_{e_{exp}} - q_{e_{cal}}/q_{e_{exp}}\right\|}{N} X\ 100$	(24)
Sum of squared error	$\mathrm{SSE} = \sum_{\mathrm{i=1}}^{\mathrm{N}} \left(\mathrm{M_{exp}} - \mathrm{M_{pre}}\right)^2$	(25)
Root mean square error	$RMSE = \sqrt{\frac{1}{N-2}\sum_{i=1}^{N}\left(\mathrm{M_{exp}} - \mathrm{M_{pre}}\right)^2}$	(26)

Hybrid fractional error function	$HYBRD = \sum_{i=1}^{N} \frac{(M_{exp} - M_{pre})^2}{M_{exp}}$	(27)
Normalized standard deviation	$NSD = 100 \times \sqrt{\frac{\sum_i^N [(q_e \exp - q_e cal)/q_e exp]^2}{N-1}}$	(28)
Chi-square test	$x^2 = \sum_{N=1}^{N} \frac{(q_{e,exp} - q_{e,cal})^2}{q_{e,cal}}$	(29)

Where N is the number of experimental runs; M_{exp} is the experimental values for the modeling; M_{pre} is the model predicted value; $M_m$is the experimental mean value, $q_{e,exp}$ and $q_{e,cal}$ are the experimental values and model calculated values respectively.

These error functions were used to investigate the accuracy of the models in predicting the removal of CR from aqueous solutions by the adsorption process. The significance of the sum of squared errors (SSE), average percentage error (APE), Hybrid fractional error function (HYBRID), and Root mean square error (RMSE) models was based on the fact that the smaller the values of the result, the better the system, while the correlation coefficient (R^2) is that the higher the value of the result to unity, the better the system.

2.13 Dissolve Salts and Solid Analysis

This analysis was carried out using a DDS-307A conductivity meter. The conductivity meter displays both electrical conductivity (EC) and total dissolution solids (TDS) results. This meter possesses a temperature sensor and conductivity probe. The probe is labeled with a cell constant. Before every measurement, the probe tip was rinsed with distilled water and the sample, and after immersing the conductivity probe into the sample for a measurement, the sample was stirred with a glass bar to achieve an ideal condition for an accurate answer.

2.13 Chemical Oxygen Demand (COD) Analysis

This analysis was carried out using Lovibond water testing RD 125 and Lovibond water testing Photometer-System MD 200. The RD 125 is the reactor used to digest the vial after mixing each with 2 ml of the samples and one with distilled water used as a blank for 120 minutes at a temperature of 150 °C or less.

2.10 Adsorbent Recycling/ Regeneration

Recycling is the process of processing materials that would have otherwise been thrown away as trash into new products, which minimizes production costs as well. This phenomenon in the adsorption process is termed desorption. Desorption is simply using an eluent to create sorption equilibrium or destabilize the bond between the pollutant (bulk phase) and the adsorbing surface. Different desorption methods, including chemical regeneration, thermal regeneration, thermochemical regeneration, steam regeneration, bio-regeneration, vacuum regeneration, electrochemical regeneration, pressure swing regeneration, ozone regeneration, microwave regeneration, oxidative regeneration, and ultrasound regeneration, have been used in the regeneration or recycling of adsorbents. In this research, a chemical regeneration method was employed, and the eluents used were acid and base.

2.10.1 Batch desorption.

The exhausted adsorbent was mixed with the eluent and stirred at a specific temperature for 30 minutes per cycle until equilibrium was reached. It was then filtered into filtrate and residue adsorbent at the end of each cycle. The filtrate was for dye analysis using a UV spectrophotometer for desorption efficacy, while the residue sorbent was washed with water to remove the eluting agent, which was then oven dried and kept for reuse in a fresh process. The amount (quantity) in mg/g and efficacy in % of desorbed adsorbate (pollutant) were calculated using equations (30) and (31), respectively.

Amount /quantity desorbed (mg/g) =$A_{des} = \frac{C_s * V}{M}$ (30)

Efficiency of desorbed (%) = $\%_{des} = \frac{A_{des}}{C_{ad}} X\ 100$ (31)

Where, C_s is concentration of adsorbate desorbed in mg/g, C_{ad} is concentration of adsorbate adsorbed in mg/g, M is weight of exhausted adsorbent in gram and V is volume of the eluent in liter.

3.0 Results and Discussion

3.1 Characterization Result

3.1.1 FTIR analysis

Fig. 1a, b, and c presents the FTIR spectra of raw Awka clay (RUC), acid modified (HCl) Awka clay (AMAC) and CR adsorbed on AMAC. From spectra of Fig.1a and 1b shows a lesser peaks at the functional region that at the finger print region. The observe peaks were all strong broad and sharp peaks of both polar groups (OH, NH, and C=O) and non-polar groups (C=C and C≡C). The higher no of these peaks was observed in Fig 1a than in Fig.1b and change in wavenumbers was also observed which may be attributed as a result of acid modification that removes impurities contained in the raw clay material and the peaks of Fig.1b composed of various functional groups which are responsible for binding of CR dye e.g. Amide, alkane, alcohol, alkyne halide. Fig.1c also showed spectra of higher peaks than Fig.1b as well which indicate the possible involvement of some functional groups on the surface of the AMAC in the adsorption process.

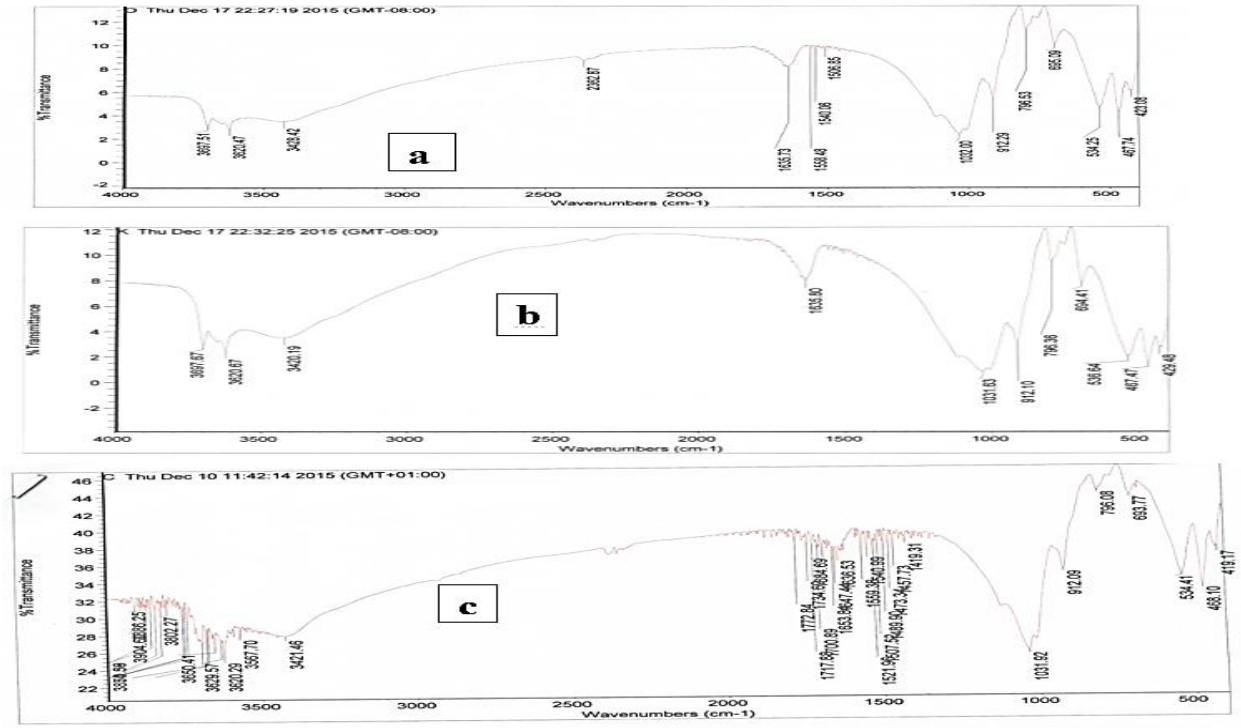

Fig.1 FTIR spectra of (a) raw clay (b) activated and (c) used clay.

3.1.2 SEM micrographs

Fig. 2a, b, and c present the scanning electron micrograph (SEM) of Awka clay samples at raw state, activated state and after CR adsorption on AMAC state. Fig. 2b clearly displayed considerable number of heterogeneous layer of pores and internal surface of the clay material than Fig. 2a, this observed development is as a result of modification which exposed the internal surface of the clay sample. Fig. 2c showed a smoother surface which signified adsorption been taken place. The observed smooth surface is dye particles that cover most porous surfaces of Fig. 2b.

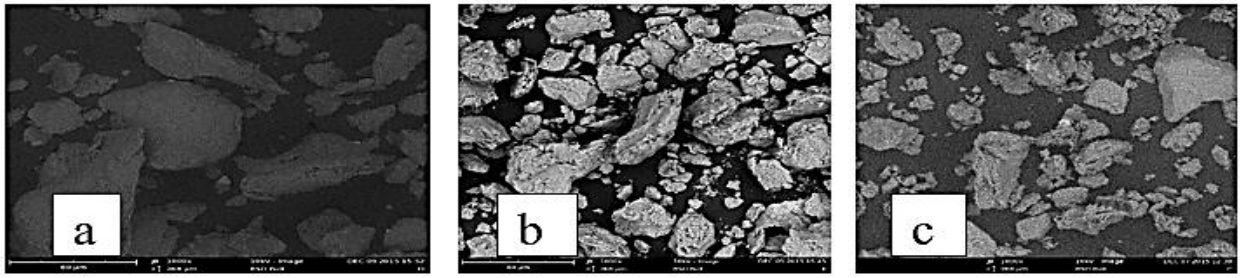

Figure 2. SEM Micrograph of: (a) raw clay, (b) activated clay, (c) after adsorbed clay

3.2 Batch Adsorption Result

3.2.1 Effect of adsorbent dosage

The adsorbent dosage effect was investigated for the dosage range of 0.2, 0.4, 0.6, 0.8, and 1g at a constant temperature of 313 k, an adsorbent particle size of 150 µm, a pH of 2, an initial dye concentration of 100 mg/l, and a time of 60 min. The result of the study, as reported in the histogram of Fig. 3A, shows that the percentage of adsorption increases with an increase in adsorbent dosage, from 53.1% at 0.2g to 97.6% at 1g. The noted rise in the percentage of dye adsorption with the increase in adsorbent dosage can be attributed to the expanded surface area of active functional groups, which leads to a higher number of available adsorption sites. (Oguanobi et al. 2024d; Imessaoudene et al. (2023)). Moreover, as the adsorbent dosage increased, a significant decrease in the amount adsorbed per unit mass of the adsorbent was observed. This decrease in unit adsorption as adsorbent dosage increases is a result of adsorption sites remaining unsaturated during the adsorption process. The result of this research concurs with the previous reports by Ismat et al. (2023) and Oguanobi et al. (2018), who reported that an increase in HAC dosage drastically decreased the amount of crystal violet dye in the aqueous solution.

3.2.2 Effect of particle size

The particle size effect was investigated with particle sizes ranging from 75, 150, 300, 600, and 850 µm at a constant temperature of 323 k, an adsorbent dosage of 1 g, an initial dye concentration of 100 mg/l, a time of 60 min, and a pH of 2. The result of the study, as reported in the histogram of Fig. 3B, shows that the percentage dye adsorption increases with sorbent size, from 60.4% at 850 µm to 98.1% at 75 µm. This is because smaller particles possess a larger surface area and pores than bigger particle sizes. Additionally, the breaking of larger particles opens tiny cracks and channels on the particle surface of the material, resulting in more accessibility and easy diffusion due to the smaller particle size. The outcome of this study concurs with the previous report by Oguanobi et al. (2018), who confirmed that an increase in adsorbent particle size distinctly decreased the percentage of dye removed.

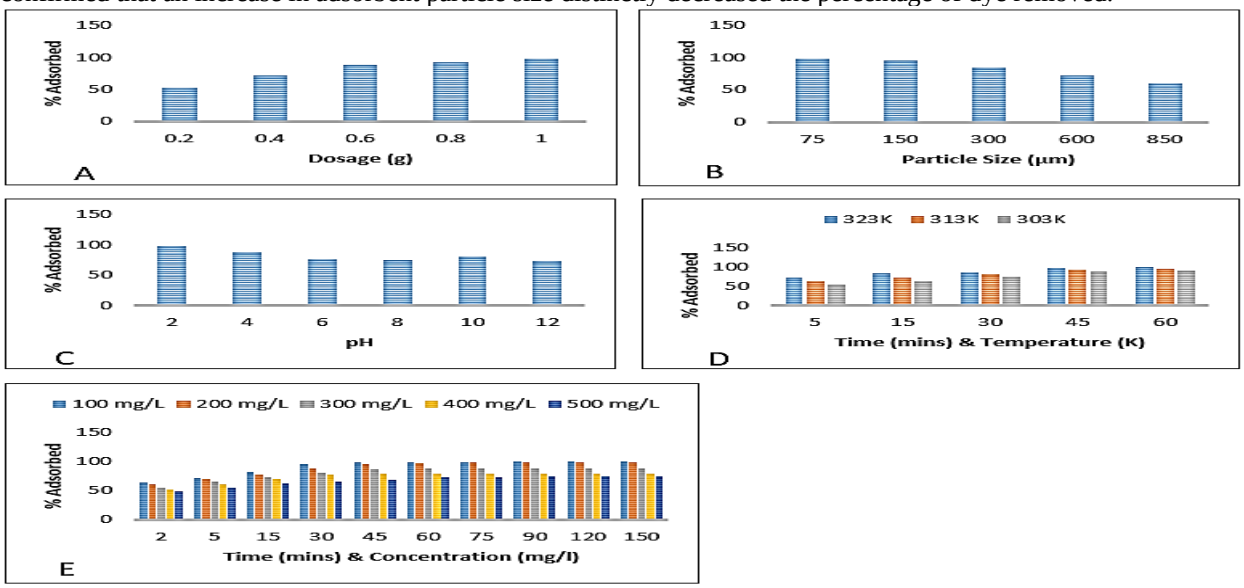

Figure 3. Effects of process parameters displaying impact of (a) particle size, (b) dosage, (c) concentration, (d) pH, and (e) temperature on the percentage of CR adsorbed

3.2.3 Effect of pH

The pH effect is paramount when the adsorbing molecules are capable of ionizing in response to pH. CR is a diazo/anionic dye and maintains its red color at pH 5, while below pH 2, the solution changes from red to dark blue; at pH 3, it changes to blue-violet; and the original red color is different above pH 10. The pH effect is studied between the pH ranges of 2 and 12, at a constant temperature of 323 k, an adsorbent particle size of 75 µm, an initial dye concentration of 100 mg/l, a time of 60 min, and an adsorbent dosage of 1g. The result of the study, as reported in the histogram of Fig. 3C, shows that the highest removal efficiency of 98% was achieved at pH 2, 80.5% at pH 10, and 73% at pH 12. These outcomes are due to the very low solubility of CR at pH < 2. Low pH leads to an increase in H^+ ion concentration in the system, and the surface of the clay acquires a positive charge by adsorbing H^+ ions. As the clay surface is positively charged at a low pH, a significantly strong electrostatic attraction appears between the positively charged sites and the anionic dye molecules. A negatively charged surface site on the clay

does not favor the adsorption of anionic CR molecules due to electrostatic repulsion. The findings of this study concur with previous reports by Imessaoudene et al. (2023) who found that pH 2 was optimal for removing Congo red using CHCFe. Popoola et al. (2021) reported optimum pH 3 for the removal of Congo red using synthesized coal graphene and activated coffee waste. Moreover, Mahmoud et al. (2019) reported that the PNP adsorption on montmorillonite is pH-dependent.

3.2.4 Effect of temperature

Temperature as a process variable studies the adsorption thermodynamics and nature, i.e., whether a system is an exothermic or endothermic process. The impact of temperature on CR uptake was examined using a temperature range of 303K, 313K, and 323K at a constant adsorbent dosage of 1g, an adsorbent particle size of 75 µm, an initial dye concentration of 100 mg/l, a pH of 2, and a time period of 60 minutes. The result, as reported in the histogram of Fig. 3D, shows an increase in the amount of CR uptake from 91.7% to 99.2% as the temperature of the solution increases. This outcome confirms the adsorption process of CR on AMAC as an endothermic system. The observed increase in CR uptake is a result of an increase in the mobility of dye molecules, which may also cause enlargement and disintegration of the internal structure of the adsorbent, thereby enabling large dye molecules to penetrate further. The obtained result is in harmony with the previous report by Oguanobi et al. (2018), who reported that CV^+ adsorption on HAC is more energetically favorable to occur at higher temperatures. Mahmoud et al. (2019) also reported similar results of the same trend.

3.2.5 Effect of concentration and contact time

The effect of initial dye concentration was studied at concentration ranges of 100–500 mg/l per 1 g adsorbent dosage at a contact time range of 150 minutes at a constant temperature of 323 k, an adsorbent particle size of 75 µm, and pH 2. The result, as reported in Fig. 3E, shows that the amount of CR adsorbed per unit mass increased with an increase in initial ion concentration from 19.99992 mg/g at 100 mg/l to 70.7741 mg/g at 500 mg/l, whereas the adsorption percentage decreased from 99.99% at 100 mg/l to 70.77% at 500 mg/l. This outcome is due to the proportion of the initial number of dye molecules to the available surface area at low concentration. Moreover, an increase in the amount or percentage of adsorption as contact time increases at all initial concentrations until equilibrium was observed (from 63.3% at 2 mins to 99.99% at 120 mins). This accounts for the driving force provided by the initial dye concentration to overcome the resistance to the mass transfer of dye between the adsorbate and the adsorbent. Finally, a three-step stage was observed during the adsorption reaction: the bulk diffusion stage (a rapid initial adsorption), the pore diffusion and intra-particle diffusion stage (a period of slower uptake), and the equilibrium stage (a period of no significant uptake). The findings of this study are consistent with those of Barakan et al. (2019) and Oguanobi et al. (2018), who found that at higher ion concentrations of As (V) and CV^+, adsorption efficiency decreased due to a decrease in available active sites. Mahmoud et al. (2019) also reported that the equilibrium of the PNP adsorption on the montmorillonite clay was reached after 120 min.

3.3 Equilibrium Modeling

The equilibrium adsorption represents the relationship between the mass of adsorbate adsorbed per unit weight of adsorbent and the liquid-phase equilibrium concentration of the adsorbate. The non-linear expression of Langmuir, Freundlich, Temkin, Vieth-Sladek, Dubinin-Radushkevich, Redlich-Peterson, and Jovanovic isotherms was used to analyze equilibrium results. The result in graphical form is reported in Fig. 4. The respective constants of each model were evaluated using software and tabulated in Table 3.

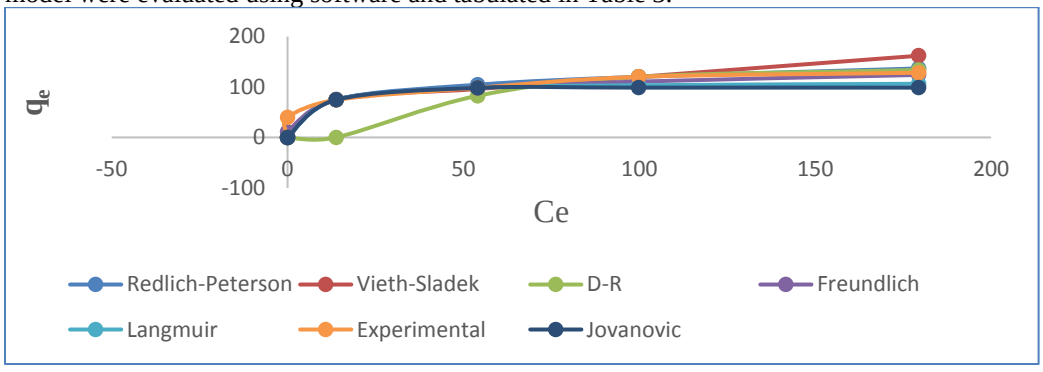

Fig.4. Non-linear isotherm plot for adsorption CR on AMAC.

From Table 3, it's seen that Langmuir maximum adsorption capacity (Q_m) value is 87.21. The K_L Value of 0.0447 indicates that the adsorbate molecules have a high affinity for the adsorbent surface (strong adsorption) and the R_L value of 0.04279 as seen in Table 3, certifies favorable uptake of CR dye.

Table 3: Isotherm and Kinetic Parameters for CR Uptake on AMAC

Langmuir	Freundlich	Temkin	D-R	V-S	Jovanovic	R-P
NSD=4.8843	NSD=4.8843	NSD=6.0521	NSD=8.8118	NSD=1.1454	NSD=5.9218	NSD=3.0607
RMSE=2.7590	RMSE=1.2912	RMSE=5.3050	RMSE=1.7165	RMSE=0.1987	RMSE=1.3209	RMSE=4.7246
X^2 =3.9x10^{-6}	X^2 =0.0014	X^2 = -	X^2 = -	X^2 = -	X^2 =0.6605	X^2 = -
APE=3.9075	APE=2.2408	APE=4.8417	APE=7.0494	APE=0.9163	APE=4.4375	APE=2.4486
q_{Max} =87.21	KF=21.5447	a_T=288.57	q_{Max} =77.063	q_{Max} =45.83	q_{Max} =67.86	Kg=52.9918
Kl=0.0447	nf=3.9367	A_T=14.7166	bdr=0.000178	Kvs= 0.2191	Kj=0.0438	aR =1.1241
RL=0.04279	1/n= 0.2540	-	E=52.95	bvs=19.99	-	g=0.9283

PFO	PSO	PNO	Avrami	Fractional	Elovich
NSD=0.1667	NSD=1.9954	NSD=0.7033	NSD=0.0438	NSD=3.9612	NSD=1.8576
RMSE=0.0288	RMSE=0.3254	RMSE=0.1475	RMSE=0.0221	RMSE=0.8341	RMSE=0.1465
X^2 =0.0014	X^2 =0.0309	X^2 =0.0104	X^2 =0.0000404	X^2 =0.1706	X^2 =0.6605
APE=0.1381	APE=0.4340	APE=0.2968	APE=0.0509	APE=1.1366	APE= -
ho=2.3592	ho=6.2408	n=3.0015	nav=0.2371	V=0.0672	B=0.323
K_1 =0.1193	K_2 = 0.0156	kn=0.0498	Kav=0.4838	K=13.7320	A=82.338
q_e =19.7793	q_e =19.9926	q_e =19.8589	q_e =19.9190	-	-

The Freundlich equation is an empirical relationship between the amounts of adsorbate molecules adsorbed onto heterogeneous surfaces. From table 3, the n_f value of 3.9367 indicates that the adsorption sites have uniform energies and thereby classify the surface as more homogeneous. The obtained n_f value also confirms the uptake of CR dye as a favorable and physical process. The high n_f value of 3.9367 confirms good affinity of the adsorbate for the adsorbent.

The Temkin model studies the adsorbate-adsorbent interaction on surfaces and the heat of adsorption. From Table 3, a high a_T value of 288.57 indicates a greater decrease in adsorption energy with increasing surface coverage, which means stronger interactions between the adsorbate and the adsorbent, whereas a significant A_T value of 14.72 indicates a broader distribution of adsorption energies, suggesting that the adsorption process involves various energy levels.

The Vieth-Sladek isotherm is used for estimating diffusion rates in solid materials from transient adsorption. From Table 3, a significant k_{vs} value of 0.2191 certifies that the adsorbent has a strong affinity for the gas molecule, whereas a significant b_{vs} value of 19.99 suggests good interaction between adsorbed molecules. The Dubinin-Radushkevich (D-R) isotherm is a temperature-dependent model that forecasts the adsorption mechanism. An adsorption process is physical when the "E" value is below 8 KJ mol^{-1} and chemical, when the "E" value is within the range of 8–16 Kj mol^{-1} (Kausar et al. 2013). From Table 3, the "E" value of 52.96 lies within the range 0-8 KJ mol^{-1} thereby confirming the uptake process of CR dye physical adsorption. The b_{DR} value of 0.000178 in Table 3 is very small, thereby suggesting a narrow energy distribution and probably a possible homogeneous system.

The Redlich-Peterson model embodied both the Freundlich and Langmuir isotherm features. From Table 3, the g value of 0.9283 suggests monolayer adsorption on a homogeneous adsorbent surface. The g value also suggests that the gas deviates more from ideal gas behavior to a real gas due to stronger intermolecular forces. This is because the deviation from ideal behavior is more pronounced. The a_R value of 1.1241 indicates that the adsorbent has a good ability to adsorb and retain more adsorbate molecules at a given temperature. The K_R value of 52.9918 indicates that the adsorbent has a great adsorption capacity and affinity for the adsorbate.

The Jovanovic model presumes superficial adsorption and mechanical interaction between the adsorbate and the adsorbent surface. The K_J value of 0.0438 indicates good adsorption affinity of the adsorbate for the adsorbent.
The high q_{max} values of Langmiur, D-R, Vieth-Sladek, and Jovanovic validate the outcome of other parameters likeK_L, $K_{R,}$, n_f, and K_J which confirm the good affinity of the adsorbent for the adsorbate.

3.4 Kinetic Modeling

Adsorption kinetics refers to the study of the rate (how fast or slow) at which an adsorbate (a gas molecule) is adsorbed onto an adsorbent (a solid surface) under specific conditions. To assess the adsorption kinetics of CR onto AMAC, various kinetic models including pseudo-first-order, pseudo-second-order, Elovich, fractional power, Avrami, and pseudo-nth-order were employed to analyze the experimental data. These pseudo-kinetic models operate under the assumption that adsorption behaves like a pseudo-chemical reaction. The Elovich model is typically utilized when chemisorption is involved in the adsorption processes (Dotto and Pinto 2011). The fitted curves for these models can be found in Fig. 5, and the values of the constants for the non-linear model were calculated using Excel software and are listed in Table 3.

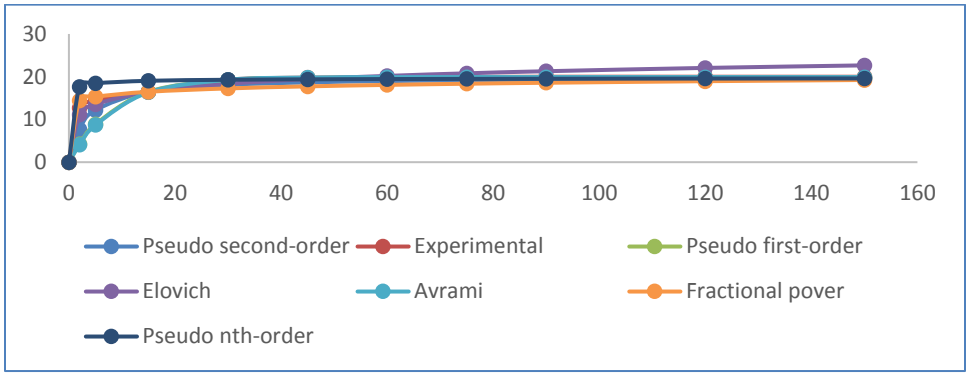

Fig.5.Non-linear kinetic plot for adsorption of CR on AMAC. (A plot of q_t against t)

From Table 3, the smaller K_1 value of 0.1193 for pseudo-first order suggests a slow adsorption process, while the smaller K_2 value of 0.0156 for pseudo-second order confirms zero correlation with the dye initial concentration, indicating that more than one adsorption mechanism controls the uptake of CR. The pseudo-nth-order constant "n," which provides information on the reaction order, and a smaller n value of 3.0015 suggest that the rate of reaction of the reactant concentration is likely to change. The smaller K_n value of 0.0498 indicates a slower reaction rate. This outcome is in agreement with the prediction of the K_1 parameter of pseudo-first order, which confirms a slow adsorption process. The H_o constant of pseudo-first and second order calculates the initial adsorption rate, and 2.3592 of PFO and 6.2408 of PSO obtained theoretically concur with the experimental date. The qe values of the PFO, PSO, PNO, and Avrami models, as tabulated in Table 3, were in agreement with those of the experimental data. The Elovich model constant "B" stands for desorption constant. The B value of 0.3723 indicates that the adsorption of CR onto AMAC is almost irreversible. The higher A value of 82.34 suggests a faster initial adsorption rate, meaning that AMAC has a high affinity for CR dye. This outcome concurs with the initial first step of the adsorption process, the "external surface adsorption or a rapid initial adsorption," as classified by Weber-Morris.

3.5 Error Function Statistical Analysis

The best fit of the studied model for the uptake of CR dye on AMAC was evaluated using the error parameters of the non-linear regression expression of equations 24, 26, 28, and 29 for equilibrium and kinetic model assessment. In non-linear regression, the rule for goodness of fit assessment is that the smaller the obtained value of the error function, the better the curve fits. The obtained results of the studied error functions for equilibrium and kinetic models, as tabulated in Table 3, show that the Vieth-Sladek model among the studied equilibrium models gives the best fit to the experimental isotherm data, as indicated by the NSD, RMSE, and APE error parameters. Additionally, the Langmuir model shows a satisfactory fit to the experimental data via the error parameter X^2. Consequently, the error parameter X^2, as shown in Table 3, cannot describe the assumptions of the D-R, V-S, R-P, and Temkin models. The Avrami model among the studied kinetic models gives the best fit to the experimental kinetic data, as indicated by the NSD, RMSE, X^2, and APE error parameters. Therefore, the Vieth-Sladek and the Avrami models are the best-fit equilibrium and kinetic models for the uptake of CR dye on AMAC after both models conform to the rule of non-linear regression. The good fit of the Avrami models was validated by the calculated qe value, which is in close agreement with the experimental data.

3.6 Adsorption Mechanism

The intra-particle diffusion model was proposed by Weber-Morris to identify the adsorption mechanism and predict the rate-controlling step. The intercept of the linear plot of qt versus $t^{1/2}$ in (mg g-1) signals an idea about the

thickness of the boundary layer, and the larger the value of the intercept, the greater the boundary layer effect (Srivastava et al. 2006). If the plot is linear and passes through the origin, then intra-particle diffusion is the rate-controlling step but if the data exhibit multi-linear plots, then two or more steps influence the sorption process. The intra-particle diffusion model can be expressed as follows:

$$q_t = K_{id}\sqrt{t} \quad (32)$$

Where q_t (mg/g) is the amount of adsorbate adsorbed at time t, and k_{id} ($mgg^{-1}min^{1/2}$) is the intraparticle constant obtained from the slope of q_t versus $t^{1/2}$.

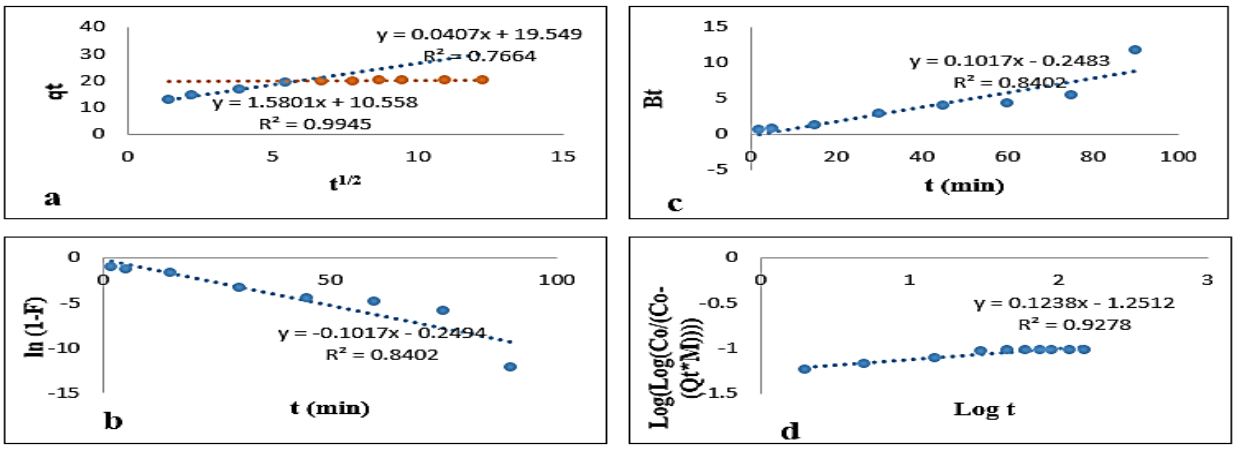

Figure 6. Adsorption mechanism plot of different model (a) Intra-particle diffusion plot, (b) Liquid film model plot, (c) Boyd diffusion model plot, and (d) Bangham model plot

Fig. 6a shows that the linear plot did not pass through the origin, which indicated that the intra-particle diffusion was not the only rate-controlling step and that the boundary layer diffusion controlled the adsorption to some degree. This deviation may be due to the difference in mass transfer rate in the initial and final stages of adsorption. Furthermore, the data, as seen in Fig. 8a, exhibit multi-linear plots, which indicates that two or more steps influence the sorption process. Comparing the k_{id} values for the macropore and micropore diffusion stages for CR uptake shows that the rate-limiting step is the micropore diffusion stage because the micropore diffusion constant $k_{id}2$ value of 0.047 is lower than the macropore diffusion constant $k_{id}1$ value of 1.5801. This outcome confirmed the rate of micropore diffusion as the slower step and the rate-determining step. Moreover, the higher value of $k_{id}1$ also indicates that the uptake of CR onto AMAC was primarily controlled by the intraparticle diffusion model. The boundary layer effect, i.e., the intercept of the micropore diffusion stages from Figure 8a, is 19.55, which further shows a greater effect than the macropore stage with an intercept of 10.56. The non-zero intercept of the macropore diffusion stage and the micropore diffusion stage clearly shows that intra-particle diffusion is not the slowest of the rate processes that determines the overall order; thus, it can be stated that the intra-particle diffusion process is not the rate-limiting step occurring during the sorption of CR onto AMAC.

Liquid film diffusion model

Liquid film diffusion model was also used in this study to investigate if transport of dye from the liquid phase up to the solid phase boundary also plays a role in the adsorption process. The Liquid film diffusion model can be expressed as follows:

$$-\ln(1-F) = -K_{fd}t \quad (34)$$

Where F is the fraction of solute adsorbed at equilibrium, K_{fd} is the liquid film diffusion constant, and F value can be evaluated using

$$F = \frac{q_t}{q_e} \quad (35)$$

Where q_t and q_e are the amount dye adsorbed on the adsorbent at any time *t* and at equilibrium respectively.

A linear plot of ─ ln (1─F) versus t with zero intercept would suggest that the kinetics of the sorption process was controlled by intra-particle diffusion through the liquid surrounding the solid sorbent.

Fig. 6b shows that the intercept of the liquid film plot of 0.2494 is close to zero, which confirms the significance of liquid film diffusion in the rate determination of the adsorption process, and the kinetics are likely to be diffusion-limited (Srivastava et al. 2006). Additionally, the higher value of the liquid film coefficient of regression (R^2) of 0.8402 indicates that film diffusion was involved in the adsorption process but not the rate-determining step. Moreover, the liquid film diffusion rate constant (K_{fd}) value of -0.1017 is insignificant compared with 1.5801 of the

intra-particle rate constant (k_{id}), which also confirms that the liquid film diffusion process was not the rate-limiting step occurring during the sorption of CR on AMAC.

Boyd pore model

The Boyd model is an empirical equation that also gives insight into the mechanism of adsorption. This model is applied to determine the rate-controlling step (the slow step involved) for the adsorption process. The Boyd model can be expressed as follows:

$$F = 1 - \left(\frac{6}{\pi^2}\right) exp^{(-Bt)} \quad (36)$$

$$Bt = -0.4977 - \ln(1 - F) \quad (37)$$

Where *Bt* is the function of *F* and *F* is the fraction of solute adsorbed at different times, *t*. The *Bt* values at different contact times, *t*, can be evaluated using equation 37 in the case of $F > 0.85$. The *F* value can be calculated using equation 26.

$$F = \frac{q_t}{q_e} \quad (35)$$

Where q_t and q_e are the amount dye adsorbed on the adsorbent at any time *t* and at equilibrium respectively.

Cáceres-Jensen et al. (2013) suggested that a straight-line plot of Bt versus t that starts at the origin indicates that pore diffusion governs the mass transfer rate (or particle diffusion mechanism). Conversely, a nonlinear plot or a linear plot that doesn't begin at the origin implies that film diffusion or external mass transport plays a more significant role (Cáceres-Jensen et al. 2013).

Fig. 6c shows that the Boyd plot is linear but did not pass through the origin, which demonstrated that intra-particle diffusion was not the solely controllable process and that diffusion-chemisorption might be more rational to explain the adsorption of CR dye ions on AMAC.

Bangham pore diffusion model

The Bangham pore diffusion model is an empirical model that investigate the adsorbate pore diffusion activities and it does so by calculating whether pore diffusion controls or dominate adsorption process. The Bangham model can be expressed as follows:

$$Log\ Log\left(\frac{C_i}{C_i - q_t M}\right) = Log\left(\frac{K_J M}{2.303V}\right) + \alpha Log t \quad (33)$$

Where C_i, is the initial concentration (mg/L), V (mL) is the volume of the solution, M is the mass of the adsorbent (g), q_t is the amount of adsorbate adsorbed at time t. K_J and α are Bangham pore constants which can be obtained from intercept and slope of the plot of Log(Log(Co/(Co-(Qt*M)))) versus Log t (double logarithm plot).

Fig. 6d shows that the Bangham plot gives a nonlinear curve for the dye removal, indicating that the diffusion of adsorbate into the pores of the adsorbent is not the only rate-controlling step. Additionally, the nonlinear curve indicates multiple adsorption stages, which validates the intra-particle diffusion model that has previously indicated that two or more steps influence the sorption process. The correlation coefficient value of 0.9278 obtained from the Bangham model suggests that pore diffusion was involved in CR uptake onto AMAC, and the linearity of the plot certifies that adsorbate pore diffusion is not the sole rate-controlling step.

3.7 Thermodynamic Study

The plot of In K_C versus T^{-1} of the CR adsorption process is carried out as indicated in Fig. 7b, and the slope and intercept obtained by a curve-fitting are used to calculate the ΔH and ΔS.

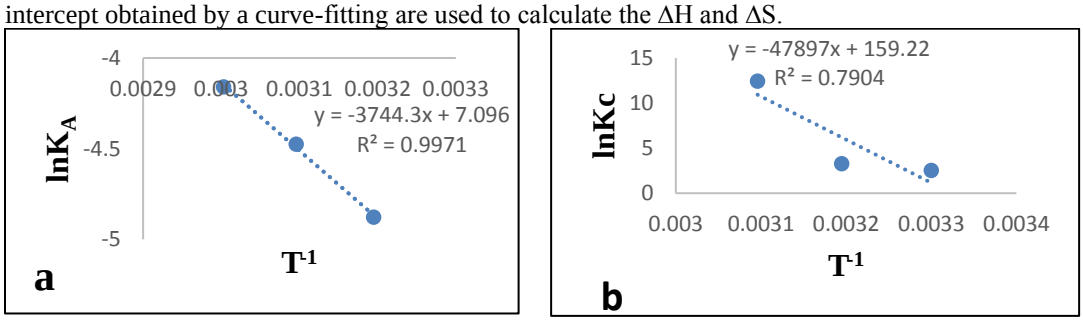

Fig.7a and b, Plot of InK_A and InK_c against T^{-1} for the removal of CR by clay adsorbent

The slope of the plots equal to $-\Delta H^o/R$ and its intercept is equal to $\Delta S^o/R$. The calculated parameters of ΔG, ΔH and ΔS are shown in Table.4.

Table 4 Thermodynamics parameters for the adsorption of CR on AMAC

Temp (K)	InK_c	ΔG (KJ/mol)	ΔS (J/mol)	ΔH (KJ/mol)	E_a (KJ/mol)
303	2.5483	-6.84317			
313	3.2797	-8.80739	1323.755	398.216	31.1301
323	12.4292	-33.3777			

The negative values of ΔG indicate that adsorption is spontaneous and the observed decrease in the obtained result of ΔG values as the temperature increases indicates that an increase in temperature favors the adsorption of CR on AMAC. The positive value of ΔH indicates that the adsorption process is endothermic, and the positive value of ΔS suggests increased randomness at the solid or solution interface during the adsorption of CR on AMAC and corresponds to an increase in the degree of freedom of the adsorbed species (Oguanobi et al 2024d).

3.7.1 Activation Energy

The magnitude of the activation energy yields information on whether the adsorption is mainly physical or chemical. The physisorption process normally had an activation energy of 5–40 KJ/mol, while chemisorption had a higher activation energy (40–800 KJ/mol) (Oguanobi et al. 2024b). In order to evaluate the activation energy of adsorption, the Arrhenius equation was applied using the relationship of Eqn. 19.

It is clearly observed from Table 4 that the E_a value for CR adsorption on AMAC is positive and below 40 KJ mol^{-1}, thus indicating that adsorption of CR using AMAC is feasible and a physisorption process. This phenomenon concurs with the Freundlich constant "n_f" result, which referred to the process as physical. A similar phenomenon was reported on the adsorption of basic dye using acid-treated kenal fiber char (Dalia et al., 2011).

3.8 Optimization and Modeling Analysis

3.8.1 RSM modeling

Design expert was used to analyze the result and the summary of P-value and the model summary statistics are presented in Table. 5.

Table 5: Statistical summary of the models investigated

Source	Df	Standard deviation	R-squared	Adjusted R^2	Predicted R^2	PRESS
Linear	4	3.70	0.5324	0.4576	0.3096	505.01
2FI	6	3.31	0.7163	0.5669	0.6010	291.84
Quadratic	4	0..0020	1.0000	1.0000	1.0000	0.0003
Cubic	8	0.0022	1.0000	1.0000	1.0000	0.0043

The quadratic model for optimum point prediction of the process was suggested from the CCD module with high R-squared, adjusted R^2 and predicted R^2 values of unity (1.0000).

3.8.1.1 ANOVA analysis for CR removal

The analysis of variance (ANOVA) confirmed the adequacy of the quadratic model.

Table 6: ANOVA and model coefficients for CR adsorption

Source	Sum of squares	df	Mean squares	F-value	p-value Prob>F
Model	731.49	14	52.25	1.316E+07	< 0.0001
A-Temperature	120.37	1	120.37	3.032E+07	< 0.0001
B-Concentration	34.95	1	34.95	8.805E+06	< 0.0001
C-pH	189.20	1	189.20	4.766E+07	< 0.0001
D-Time	44.96	1	44.96	1.133E+07	< 0.0001
AB	2.00	1	2.00	5.026E+05	< 0.0001
AC	11.58	1	11.58	2.917E+06	< 0.0001
AD	0.0018	1	0.0018	455.04	< 0.0001
BC	96.97	1	96.97	2.443E+07	< 0.0001
BD	0.2186	1	0.2186	55060.28	< 0.0001
CD	23.69	1	23.69	5.969E+06	< 0.0001
A^2	44.10	1	44.10	1.111E+07	< 0.0001
B^2	108.13	1	108.13	2.724E+07	< 0.0001

C^2	50.51	1	50.51	1.272E+07	< 0.0001
D^2	33.74	1	33.74	8.499E+06	< 0.0001
Residual	0.0001	15	3.969E-06		
Lack of fit	0.0001	10	5.954E-06		
Pure error	0.0000	5	0.0000		
Cor total	731.49	29			

Significant terms of the model are checked from F-values and P-values. The higher the F-value, the smaller the P-value, and the more significant the corresponding coefficient. The higher model F-value of 13162969.23 implies that the model is significant, and P-values less than 0.0500 indicate model terms are significant; therefore, A, B, C, D, AB, AC, AD, BC, BD, CD, A^2, B^2, C^2, and D^2 are significant terms. A similar phenomenon was reported by Oguanobi et al. (2024c). The empirical correlation between the variables (response and independent) in the coded form on the basis of the experiment results was reported as follows:

% Adsorbed = 89.87 - 1.32A + 2.45B - 3.08C - 1.50D - 0.3531AB + 0.8506AC - 0.0106AD - 2.46BC + 0.1169BD - 1.22CD -2.17A^2 - 3.40B^2 + 2.33C^2 + 1.90D^2 (34)

The good fit of the model equation was validated using R^2 (coefficient of regression). The high coefficient of regression value of unity (1) implies that 100% of the variability in the response can be explained by the model.

3.8.1.2 RSM graphical plots

The 3D surface plots represent the effect of two process variables on the adsorption of CR. Fig.8a-b, presents the relationship between every two independent process variables. The circular nature of the contour in the graphs shows that there was a perfect significance between every two variables.

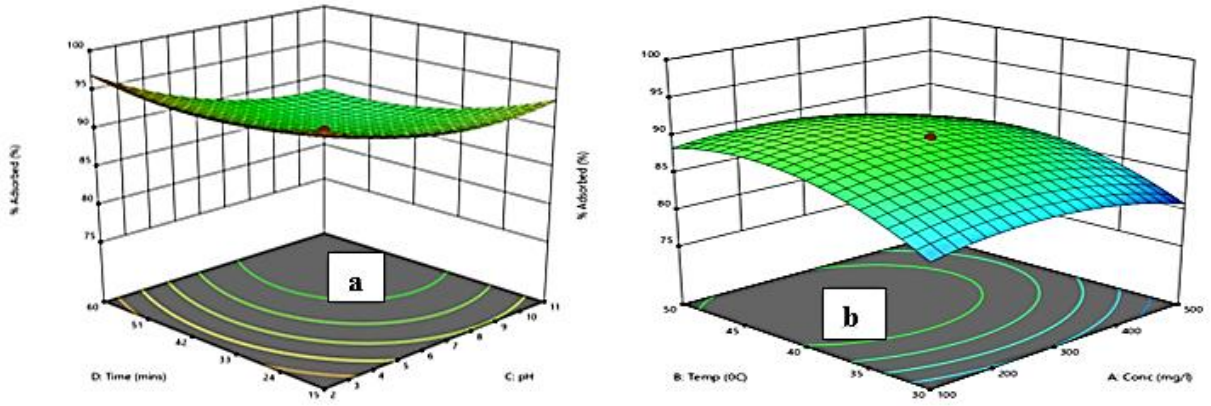

Figure 8. 3D surface plot for CR adsorption on the adsorbent showing combined effects of (a) Time and pH, (b) Temperature and concentration

Figure 8a shows that increase in adsorption reaction time along with decrease in pH led to increase in dye percentage removal when the concentration and temperature were constant etc. Figure 8b shows that increasing temperature a certain degree increases whereas increase in concentration decreases dye percentage removal when the pH and time were constant.

3.8.2 ANN modeling and prediction

The artificial neural network for the adsorption of CR was modeled using the neural toolbox of MATLAB software. The best ANN with input, hidden, and output nodes of 4, 9, and 1, respectively, was used to model the optimum percentage removal of CR in the adsorption process.

The validation of the neural network process at the 6th epoch iteration was achieved using the ANN validation performance plot in Figure 9, and the lowest mean square error of 5.57821×10^{-23} and R^2 value of 0.99999 was observed.

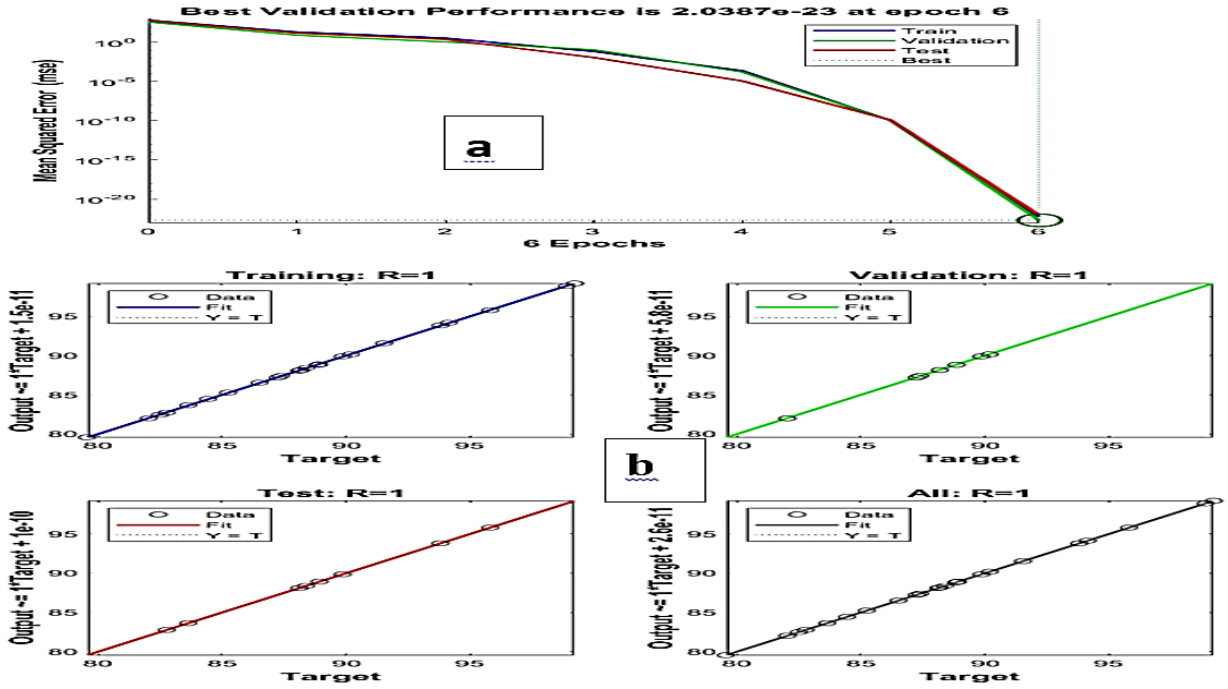

Figure 9: ANN plots for (a) validation performance and (b) regression plots for training, test, validation and overall process

The regression values of unity were obtained for the training, testing, validation, and all (overall) data, respectively as shown in Figure 9b. These coefficients of regression values of unity explain the nature of the neural fittings. Moreover, the outputs were very close to the targets, as most of the data points were assembled along the straight line of the coefficient of regression. The percentage predicted CR removal of the ANN model is presented in Table 7.

3.8.3 ANFIS modeling and prediction

The ANFIS data was trained at 5 epoch iterations with an error tolerance of zero. A minimum error of 0.0002212 was produced after the 2nd epoch, which gives reliance on the adequacy of the ANFIS model in predicting the removal of CR dye. A correlation coefficient of 0.9999 confirms the adequacy of the ANFIS model in predicting the removal of CR dye from wastewater using Awka clay.

3.8.4 Comparison of Experimental Response with Predicted Response of RSM, ANN, and ANFIS models

Table 7: Experimental and predicted results for CR removal

Conc (mg/l)	Temp (0C)	pH	Time (mins)	Exp. Response	RSM Pred. Response	ANN Pred. Response	Anfis Pred. Response
100	30	2	15	88.89	88.89	88.89	88.89
500	30	2	15	85.27	85.27	85.27	85.27
100	50	2	15	99.19	99.19	99.19	99.19
500	50	2	15	94.16	94.16	94.16	94.16
100	30	11	15	88.39	88.39	88.39	88.39
500	30	11	15	88.18	88.18	88.18	88.18
100	50	11	15	88.85	88.85	88.85	88.85
500	50	11	15	87.22	87.22	87.22	87.22
100	30	2	60	88.11	88.11	88.11	88.11
500	30	2	60	84.45	84.45	84.45	84.45
100	50	2	60	98.88	98.88	98.88	98.88
500	50	2	60	93.81	93.81	93.81	93.81

100	30	11	60	82.75	82.75	82.75	82.75
500	30	11	60	82.49	82.49	82.49	82.49
100	50	11	60	83.67	83.67	83.67	83.67
500	50	11	60	82	82	82	82
17.16	40	6.5	37.5	87.39	87.39	87.39	87.39
582.8	40	6.5	37.5	83.65	83.65	83.65	83.65
300	25.86	6.5	37.5	79.59	79.59	79.59	79.59
300	54.14	6.5	37.5	86.53	86.53	86.53	86.53
300	40	0.136	37.5	98.87	98.87	98.87	98.87
300	40	12.86	37.5	90.17	90.17	90.17	90.17
300	40	6.5	5.68	95.79	95.79	95.79	95.79
300	40	6.5	69.3	91.55	91.55	91.55	91.55
300	40	6.5	37.5	89.87	89.87	89.87	89.87
300	40	6.5	37.5	89.87	89.87	89.87	89.87
300	40	6.5	37.5	89.87	89.87	89.87	89.87
300	40	6.5	37.5	89.87	89.87	89.87	89.87
300	40	6.5	37.5	89.87	89.87	89.87	89.87
300	40	6.5	37.5	89.87	89.87	89.87	89.87

The result showed that the three models were good at modeling and predicting the removal of CR from wastewater in an adsorption process. RSM with the lowest residuals in most experimental data sets seems to be the best at predicting the percentage of CR removed. Further statistical analyses were used to compare the adequacy of the three models in Table 8.

Table 8: Comparative statistical analysis of RSM, ANN, and ANFIS models

Model parameter	RSM	ANN	ANFIS
R^2	1	0.99999	1
APE	0	$1.8x10^{-13}$	$7.2x10^{-6}$
HYBRID	0	$8.03x10^{-24}$	$1.2x10^{-8}$
RMSE	0	$5.2x10^{-12}$	$2.07x10^{-4}$
SSE	0	$2.1x10^{-20}$	$3.4x10^{-5}$

The model parameters investigated include R^2, APE, HYBRID, RMSE, and SSE. In the model indices, ANFIS showed the least modeling predictive ability in four of the studied error functions used for the comparative analysis, except in R^2 where ANN exhibited the least modeling predictive ability. RSM exhibited zero error when compared with the experimental data of CR dye removal from wastewater, thereby confirming the best predictive model.

3.9 Comparative Performance of the Adsorbent

A comparison of the adsorption of Congo red dye with other adsorbents was made to ascertain the efficiency and relevancy of the modified clay used in this study. Maximum adsorption capacity (q_{max}), percentage removal, and adsorbent dosage were the parameters utilized in the comparison, as shown in Table 9.

Table 9: Comparison with other adsorbents

Adsorbent	Adsorbent dos (g)	Removal eff (%)	Ads capacity(mg/g)	Adsorbate	Reference
Pottery clay	0.05	94.75	1.086	Congo red	Baydaa and Lekaa (2022)
MgAl-LDH	0.05	60	769.23	Congo re	Mohamed et al. (2022)
PDFe/Al	1	99	411	Congo red	Khathutshelo et al. (2022)
glAMAConite	0.02	80	11.9	Congo red	Hamd et al. (2023)
Treated clay	0.3	90	39.80	Heavy metals	Paul and Mutsee (2021)
Raw clay	0.5	64.99	25.99	Crystal violet	Oguanobi et al. (2024a)
Banana stem	0.5	87	14.28	Remazole red	Kumar et al. (2022)
Rice bran	2	97.4	603	Crystal violet	Mojtaba et al. (2020)

Fe-bent	2	99	10.06	Arsenic(v)	Barakan et al. (2019)
AUC	0.5	99.99	140.5	Congo red	Oguanobi et al. (2024c)
AMAC	1	99.99	19.99	Congo red	Present study

From table 9, it can be seen that the adsorption capacity and removal efficiency of the modified Awka clay was higher than some of the reviewed adsorbents. The available of this clay in large deposit in Awka town, Nigeria with its adsorption efficiency makes it a viable effective and alternative adsorbent in the removal of Congo red dye from contaminated water. Moreover, irrespective of negative implications of clogging and fouling of treatment system which invariably increases maintenance cost, and disposal challenges, AMAC effectiveness in removal of CR and other contaminants as seen in the results of this study together with its natural, non-toxic and bio-degradable nature makes it an environmental eco-friendly option for dye removal.

Table 10 Comparison of parameters of untreated and treated simulated industrial wastewater containing CR dye after 24hrs incubation

Parameters	Wastewater	Treated Wastewater	% Removal
EC (µs/cm)	101	17.4	83.17
TDS (mg/l)	51	3.8	92.55
COD (mg/l)	169	32	81.07
Color removal (mg/l)	100	0.0004	99.99

Table 10 presents the adsorption capacity and removal efficiency of the AMAC in minimizing contamination of dye industrial wastewater. The obtained result shows a high reduction rate of the tested parameters after treatment, which thereby confirms AMAC as a reliable adsorbent for which its use in wastewater treatment will provide sustainability like low-cost water treatment, local economic growth, improved livelihood, job creation, increased food security, and improved public health in underdeveloped countries. The obtained result is in agreement with the previous report by Mustafa et al. (2023), who reported that the biosynthesis of nickel oxide nanoparticles removes 48.38% of EC, 49.24% of COD, and 67.05% of TDS from azo dye industrial wastewater.

3.10 Regeneration of Adsorbent

The reusability capacity of the adsorbent was presented in Fig. 16A-C. Fig. 16A presents the effect of four different temperatures (303 k, 313 k, 323 k, and 333 k) on two different eluents (alkaline eluent and acidic eluent) after three desorption cycles. The result shows that CR dye desorption works perfectly with alkaline eluent due to the electrostatic repulsion that exits when the OH^- ion of NaOH neutralizes the H^+ ion on the surface of the adsorbent. Additionally, the result also indicates that temperature did not have a significant effect during the process; therefore, low temperatures pose the benefit of cost efficiency. Fig. 16B presents the effect of three eluent concentrations (1M, 3M, and 5M) on the desorption process. The obtained result shows that low and higher concentrations did not favor the process, since 94.5% reusability capacity was recorded at 3M concentrations against 60.1% at 5M and 77.7% at 1M concentrations after three successive regeneration cycles. The slow rate of desorption at 1M is attributed to a weak driving force and thus requires a larger volume of eluent to achieve the same objective as with mid-concentrated eluent, whereas the low desorption rate at higher concentrations is due to the adverse effect of eluent high concentration strength, which may destabilize or weaken the chemical and pore structure of the adsorbent (Oguanobi et al. 2024b). Fig.10C presents the effect of different pHs of the eluent (pH 2-12) on the desorption process. The highest reusability capacity of 97.2 was achieved at pH 10 after three successive regeneration cycles. This high reusability capacity at pH 10 instead of pH 12 is attributed to high alkalinity strength, which may weaken both the chemical and pore structures of the adsorbent surface and thereby lead to poor outcomes. This outcome validates the results of choice and concentration of eluent, which favor alkaline eluent and 3M concentration, respectively. Finally, Fig.10B shows an insignificant change in reusability capacity after the 2nd and 3rd desorption cycles, irrespective of whether the 3rd was the best. The minor change in reusability capacity is attributed to characteristics of equilibrium. The obtained result is in agreement with the previous report by Zhang et al. (2018), who reported that temperature has an insignificant effect on the desorption of the five synthetic azo dyes (tartrazine, amaranth, carmine, sunset yellow, and allura red). They also reported that optimized desorption efficiency was achieved at pH 9. Wang et al. (2020) reported similar results with the same trend on effect concentration. Himanshu (2021) reported that alkali eluents are best used for anionic adsorbates.

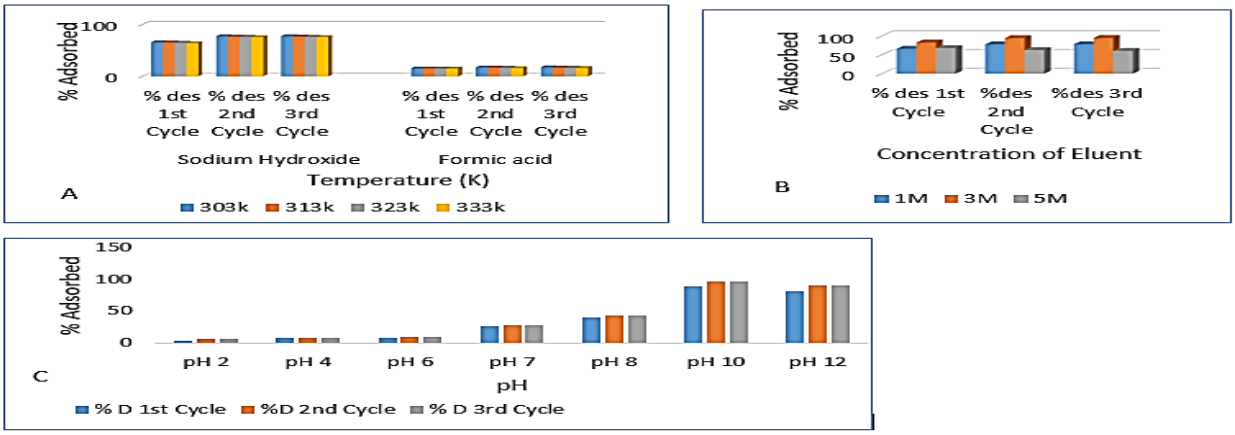

Figure 10: Effect of temperature, concentration, and pH of eluent on desorption of CR on AMAC

4.0 Conclusions

The present study established the potential of AMAC as an adsorbent for the removal of dye from aqueous solutions. The adsorption of CR onto AMAC was found to be dependent on the pH solution, initial dye concentration, temperature, adsorbent dosage, contact time, and adsorbent particle size. The equilibrium adsorption data was best represented by the V-S isotherm model. The Langmuir model produced the highest maximum adsorption capacity (q_{max}) value of 87.21 mg/g. The adsorption kinetics are best described by Avrami kinetic models. From the thermodynamic studies, the adsorption process was spontaneous, endothermic, favorable, and physical, and this was in agreement with the findings of the equilibrium adsorption parameters. The ANN, ANFIS, and RSM models were adequate for predictive modeling of the adsorption process, though the statistical analysis indicated that the RSM model was marginally better than the ANN and ANFIS. Finally, further studies on AMAC life cycle assessment and exploring hybrid treatment system combining AMAC with other materials for adsorption system or other technologies to improve its efficacy is recommended.

References

Arulkumar, M., Sathishkumar, P., Palvannan, T. 2011 Optimization of orange G dye adsorption by activated carbon of thespesiapopulnea pods using response surface methodology. *Journal of Hazardous Materials.* 186 (1), 827–834. https://doi.org/10.1016/j.jhazmat.2010.11.067.

Bahman Najafi, Sina Faizollahzadeh Ardabili 2018 Application of ANFIS, ANN, and logistic methods in estimating biogas production from spent mushroom compost (SMC). *Resources, Conservation & Recycling* 133 (2018) 169–178 https://doi.org/10.1016/j.resconrec.2018.02.025

Barakan S, Aghazadeh V, Samiee B. A, Mohammadi S. 2019 Thermodynamic, kinetic and equilibrium isotherm studies of As(V) adsorption by Fe(III)-impregnated bentonite. *Environ Dev Sustain*. https://doi.org/10.1007/s10668-019-00424-2

Baydaa N. A, and Lekaa H. K. 2022. Removal of Congo Red Dye from Aqueous Solution Using Different Clays Adsorbent. *Journal of Algebraic Statistics* Volume 13, No. 3, 2022, p. 861 - 875 https://publishoa.com ISSN: 1309-3452 861

Cáceres-Jensen L., Rodríguez-Becerra J., Parra-Rivero J., Escudey M., Barrientos L, and Castro-Castillo V. 2013 Sorption kinetics of diuron on volcanic ash derived soils. *Journal of Hazardous Materials.* 2013;261: 602–613. doi: 10.1016/j.jhazmat.2013.07.073.

Dal S. K, and Meenal G. 2022 Treatment of Textile Dyeing Effluent Using Agriculture Waste Based Adsorbents - A Review. *Chemical Science International Journal*. Volume 32 [Issue 6] DOI: 10.9734/CSJI/2023/v32i6870

Dalia, K. M; Mohamad, A. M. S; Wan, A. W. A. K; Azni, I, and Zurina, Z. A. 2011 Batch adsorption of basic dye using acid treated kenaffibre char: equilibrium, kinetic and thermodynamics studies. *Chem Eng. J.* 181-182, 449-457. Doi: 10.1016/j.cej.2011.11.116.

Dotto, G. L., and Pinto, L. A. A. 2011. Adsorption of Food Dye Acid Blue 9 and Food Yellow 3 onto Chitosan: stirring Rate effect in Kinetics and Mechanism. *J Hazard.Mater*. 187, 164-170.

Gonzalez C.R.T, Subathra M.S.P, and Manoj N.K.N. 2020 Modelling the daily reference evapotranspiration in semi-arid region of South India: A case study comparing ANFIS and empirical models. *Information Processing in Agriculture 2020;* 2-12. https://doi.org/10.1016/j.inpa.2020.02.003.

Hamd A, Salah D, Alyafei H. F, Soliman N. K, El-Reedy A. A. M, Elzanaty A. M, Al-Saeedi S. I, Al-Ghamdi A, Shaban M, and El-Sayed R. 2023. NaOH-Activated Natural Glauconite for Low-Cost Adsorption of Congo Red Dye *Water* 2023, 15, 3753. https://doi.org/ 10.3390/w15213753

Himanshu P. 2021. Review on solvent desorption study from exhausted adsorbent. *Journal of Saudi Chemical Society* (2021) 25, 101302

Imessaoudene, A.; Cheikh, S.; Hadadi, A.; Hamri, N.; Bollinger, J.-C.; Amrane, A.; Tahraoui, H.; Manseri, A.; Mouni, L. 2023. Adsorption Performance of Zeolite for the Removal of Congo Red Dye: Factorial Design Experiments, Kinetic, and Equilibrium Studies. *Separations* 2023, 10, 57. https://doi.org/10.3390/separations10010057

Ismat A. E, Marufa K, Most. Afroza K, Owaleur R.M.d., Anis-Ul-Haque K. M., and Md. Jahangir A. 2023 Removal of Dye from Wastewater Using a Novel Composite Film Incorporating Nanocellulose. *Advances in Polymer Technology* Volume 2023, Article ID 4431941, 9 pages https://doi.org/10.1155/2023/4431941

Kausar A., Bhatti H. and Mackinnom G. 2013 Equilibrium kinetic and thermodynamics studies on the removal of U (VI) by low-cost agricultural waste, *Colloids and Surface B,* Vol 111, 2013, 124-133. Doi.org/10.1016/j.colsurfb.2013.05.025.

Khathutshelo L. M., Vhahangwele M., Johannes P. M., Nils H., and Hendrik G. B. 2022. Nanotechnology in the Restoration of Polluted Soil. *Nanomaterials (Basel).* 12(5): 776. doi: 10.3390/nano12050776.

Kumar K. A, Bharath M, and Krishna B. M. 2022. Adsorption kinetics of reactive dye using agricultural waste: banana stem. *Water Practice and Technology* 17 (1): 128–138. https://doi.org/10.2166/wpt.2021.106

Mahammedi F and Benguella B., 2016 Adsorption of methylene blue from aqueous solutions using natural clay. *J. Mater. Environ. Sci*. 7 (1) (2016) 285-292

Mahmoud El O., Mohamed L., Hicham A. O., Younes B., Abdelhadi A., Abdelaziz E., Abdelaziz A. A., and Abdellatif L. 2019 Efficient removal of p-nitrophenol from water using montmorillonite clay: insights into the adsorption mechanism, process optimization, and regeneration. *Environ Sci Pollut Res* 26:19615–19631. https://doi.org/10.1007/s11356-019-05219-6

Manpreet S.B., DhritiKapoor, R.K., Kalia, A. S. R., and Ashwani K.T. 2011 RSM and ANN modeling for electrocoagulation of copper from simulated wastewater: Multi objective optimization using genetic algorithm approach. *Desalination* 274 (2011) 74–80. doi: 10.1016/j.desal.2011.01.083.

Mingyi, F., Tongjun, L., Jiwei, H., Rensheng, C., Xionghui, W., Xuedan, S., and Wenqian, R. 2017. Artificial neural network modeling and genetic algorithm optimization for cadmium removal from aqueous solutions by reduced graphene oxide-supported nanoscale zero-valent iron (nzvi/rgo) composites. Materials. 10 (544), 1 – 22. doi:10.3390/ma10050544.

Mohammed B., Mustapha D., and Ftiha D. 2022 Adsorption of dye using natural clay from water. *Journal of Environmental Engineering and Science.* Volume 17 Issue 4, December 2022, pp.175-183. https://doi.org/10.1680/jenes.21.00051

Mohammed G. H., Magdy A. W., Hosni A. G., and Ahmed S. E. 2023 Adsorption of Rose Bengal dye from waste water onto modified biomass. *Sci Rep.* 2023; 13: 14776. doi: 10.1038/s41598-023-41747-5

Muhammed O, and Çiğdem S. Ö. 2022 Equilibrium Studies for Dye Adsorption onto Red Clay. *Journal of Engineering and Natural Sciences* 3:2 2022 36-45. https://dergipark.org.tr/tr/pub/naturengs DOI: 10.46572/naturengs.1120218

Mustafa S, Mahmood F, Shafqat U, Hussain S, Shahid; Batool F, Elnour R. O, Hashem M, Asseri T. A. Y, and Shahzad T. 2023. The Biosynthesis of Nickel Oxide Nanoparticles: An Eco-Friendly Approach for Azo Dye Decolorization and Industrial Wastewater Treatment. *Sustainability* 2023, 15, 14965. https://doi.org/ 10.3390/su152014965

Nayoon C, Yeongkyun S, Tae-Hyun K, Yuri P, and Yuhoon H. 2022. Adsorption behaviors of modified clays prepared with structurally different surfactants for anionic dyes removal. *Environmental Engineering Research* 2023; 28(2): 210076. DOI: https://doi.org/10.4491/eer.2022.076

Oguanobi N. C., Onu, C. E., and Onukwuli O. D. 2019 Adsorption of a dye (Crystal Violet) on acid modified non-conventional adsorbent. *Journal of Chemical Technology and Metallurgy*, 54 (1) 95-110.

Oguanobi N.C, Calistus N. Ude, Okechukwu D. Onukwuli, Ephrem N. Anike. Chinaemezu B. Kalu. 2024c. Adsorption Kinetics of Congo Red Dye Using Acid Modified Umuahia Clay: Modeling and Optimization Analysis. *Nigerian Research Journal of Engineering and Environmental Sciences.* Accepted

Oguanobi N.C, Ude C.N, Nnaji P.C, Onukwuli O.D, Anike E.N. Okonkwo G, and Okonkwo C.H. 2024a. Adsorption Behaviors of Raw Clay for Cationic Dyes Removal: Equilibrium, Kinetic Modeling, Thermodynamics, and RSM Optimization, *Umudike Journal of Engineering and Technology.* vol. 10 No. 1, June 2024. Doi: https://doi.org/10.33922/j.ujet_v10i1_19.

Oguanobi N.C, Okonkwo. G, Onukwuli O.D, Ude C.N, Anike E.N. 2024b. Kinetic and Modeling of Anionic Dye Adsorption onto Acid modified Ihiala Clays: ANN, ANFIS and RSM comparative analysis. UNIZIK Journal of Engineering and Applied Sciences 3(2), September (2024), 867-902.

Oguanobi, N. C., Okonkwo, G., Onukwuli, O. D., Ude, C. N. and Anike, E. N. 2024d Adsorption of Anionic Dyes From Aqueous Solutions onto Natural Clay: Kinetic, Equilibrium, Thermodynamics and Modelling Analysis. Umudike Journal of Engineering and Technology (UJET); Vol. 10, No. 2, December 2024, pp. 18 – 29; https://doi.org/10.33922/j.ujet_v10i2_3

Onu C. E., Oguanobi N. C., Okonkwo C. O., and Nnamdi-Bejie J. 2020 Application of Modified Agricultural Waste in the Adsorption of Bromocresol Green Dye. *Asian Journal of Chemical Sciences.* 7(1): 15-24. https://doi.org/10.9734/AJOCS/2020/v7i119011

Paul E. D, and Mutsee T. 2021. Treated Clay Mineral as Adsorbent for the Removal of Heavy Metals from Aqueous Solution. *Applied science and engineering progress* Vol 14, No 3 https://doi.org/10.14416/j.asep.2021.04.002

Popoola, T. J., Okoronkwo, A. E., Oluwasina, O. O., and Adebayo, M. A. 2021. Preparation, characterization, and application of a homemade graphene for the removal of Congo red from aqueous solutions. *Environ. Sci. Poll. Res.* 28, 52174–52187

Sabarish R, Jasila K, Aswathy J, Jyotishkumar P, Jaewoo L, Jyothi Mannekote S, Rajarathinam N, and Suchart S, 2022 Adsorption of anionic dye onto ZSM-5 zeolite-based bio membrane: Characterizations, kinetics and adsorption isotherm. *Journal of polymers and the environment.* https://doi.org/10.21203/rs.3.rs-1191111/v1

Srivastava, V. C., Mall, I. D., and Mishra, M. 2007 Adsorption thermodynamics and isosteric heat of adsorption of toxic metal ion onto bagasse fly ash (BFA) and rice husk ash (RHA), *Chem. Eng. J.*132, 267-278.

Venkatesh P.M., and Karthikeyan R. 2018 Comparative studies on modelling and optimization of hydrodynamic parameters on inverse fluidized bed reactor using ANN-GA and RSM. *Alexandria Engineering Journal* 57:3019–3032. https://doi.org/10.1016/j.aej.2018.05.002.

Wang G., He D., Fengchun Z.F., Hu J., Lee Y., Shi J., and Xu J. 2020 Extraction and purification of ustiloxin A from rice false smut balls by a combination of macroporous resin and high-speed countercurrent chromatography. *Food Production, Processing and Nutrition* 2:29 https://doi.org/10.1186/s43014-020-00043-9

Zhang X., Zhang J., Li W., Yang Y., Qin P., Zhang X., and Lu M. 2018. Magnetic graphene oxide nanocomposites as the adsorbent for extraction and pre-concentration of azo dyes in different food samples followed by high-performance liquid chromatography analysis. *Taylor & Francis Group* https://doi.org/10.1080/19440049.2018.1526415

Zhi L., Xiaohai H., Yi M., Bing G., Yiling S., Jianghui Z., Soon H. T. 2022 Eggplant biomass based porous carbon for fast and efficient dye adsorption from wastewater. *Industrial Crops and Products*.Volume 187, Part B, 1 November 2022, 115510 https://doi.org/10.1016/j.indcrop.2022.115510Get rights and content

Zineb El K., Jaouad B., Nouhaila F., Abdelali El M., Avni B., Zaki S., Hanae O., Farid K., Musaab D., Hiba-Allah N., Abdel-Rhman Z. G., Mohammed B., Amar H., and Nouredine EL M. 2023. Physicochemical Characterization of Clay and Study of Cationic Methylene Blue Dye Adsorption. *ACS Omega* 2023, 8, 43, 40848–40863. https://doi.org/10.1021/acsomega.3c06019.